

# Understanding the role of initial soil moisture and precipitation magnitude in flood forecast using a hydrometeorological modelling system

Dongxiao Yin<sup>1</sup>  | Z. George Xue<sup>1,2,3</sup>  | Daoyang Bao<sup>1</sup> | Arezoo RafieeiNasab<sup>4</sup> | Yongjie Huang<sup>5</sup>  | Mirce Morales<sup>6</sup> | John C. Warner<sup>7</sup>

<sup>1</sup>Department of Oceanography and Coastal Sciences, Louisiana State University, Baton Rouge, Louisiana, USA

<sup>2</sup>Center for Computation and Technology, Louisiana State University, Baton Rouge, Louisiana, USA

<sup>3</sup>Coastal Studies Institute, Louisiana State University, Baton Rouge, Louisiana, USA

<sup>4</sup>Research Applications Laboratory, National Center for Atmospheric Research, Boulder, Colorado, USA

<sup>5</sup>Center for Analysis and Prediction of Storms, University of Oklahoma, Norman, Oklahoma, USA

<sup>6</sup>Faculty of Engineering, National Autonomous University of Mexico, Mexico City, Mexico

<sup>7</sup>U.S. Geological Survey, Woods Hole Coastal and Marine Science Center, Woods Hole, Massachusetts, USA

## Correspondence

Z. George Xue, Department of Oceanography and Coastal Sciences, Louisiana State University, Baton Rouge, LA 70803, USA.  
Email: [zxue@lsu.edu](mailto:zxue@lsu.edu)

## Present address

Dongxiao Yin, Department of Physical Sciences, Virginia Institute of Marine Science, William & Mary, Gloucester Point, Virginia, USA.

## Funding information

LSU Economic Development Assistantship;  
USGS The Cooperative Ecosystem Studies Units, Grant/Award Number: G20AC00099

## Abstract

We adapted the WRF-Hydro modelling system to Hurricane Florence (2018) and performed a series of diagnostic experiments to assess the influence of initial soil moisture and precipitation magnitude on flood simulation over the Cape Fear River basin in the United States. Model results suggest that: (1) The modulation effect of initial soil moisture on the flood peak is non-linear and weakens as precipitation magnitude increases. There is a threshold value of the soil saturation, below and above which the sensitivity of flood peak to the soil moisture differentiates substantially; (2) For model spin-up, streamflow needs longer time to reach the ‘practical’ equilibrium (10%) than the soil moisture and latent heat flux. The model uncertainty from spin-up can propagate through the hydrometeorological modelling chain and get amplified into the flood peak; (3) For ensemble flood modelling with a hydrometeorological system, modelling uncertainty is dominated by the precipitation forecast. Spin-up induced uncertainty can be minimized once the model reaches the ‘practical’ equilibrium.

## KEY WORDS

cape fear river basin, flood modelling, hurricane florence, initial soil moisture, precipitation magnitude, spin-up, WRF/WRF-hydro

## 1 | INTRODUCTION

Flooding is the most frequently occurring natural disaster. Around the globe, it accounts for 39% of natural hazards since 2000 and affects more than 94 million people each year (Wu et al., 2020). Flooding is the costliest natural disaster in the United States as well. Over the

past 30 years, the annual average economic loss from freshwater flooding amounts to \$8.2 billion (Wing et al., 2018). For the eastern United States, a major cause of flooding is the landfalling tropical cyclones (Smith et al., 2010; Villarini & Smith, 2010). During 1963–2012, hurricane induced inland floods and mudslides accounted for 27% out of 2325 natural disaster-related deaths in America

(Rappaport, 2014). Climate models project an increase in both the intensities of the strongest storms and the accompanying rain rates (Dinan, 2017; Knutson et al., 2010; Walsh et al., 2016). This foreseeable challenge under climate change requires better understanding and reliable flood forecasting.

Precipitation and soil moisture are well acknowledged as the two most important climate variables controlling flood response (Brocca et al., 2008; Massari, Brocca, Barbetta, et al., 2014; Massari, Brocca, Moramarco, et al., 2014). As the dominant meteorological driver, the magnitude and intensity (Diakakis, 2012; Hewlett et al., 1977; Smith et al., 2005) and spatial-temporal distribution (Huang et al., 2012; Klongvessa et al., 2018; Ogden & Julien, 1993; Oppel & Fischer, 2020; Singh, 1997; Villarini et al., 2011) of precipitation, as well as associated storm motion (Singh, 1997; Sturdevant-Rees et al., 2001; Yang et al., 2017) can all exert substantial influence on flooding. Meanwhile, soil moisture is the major variable defining hydrologic state and plays a key role in modulating rainfall-runoff processes (Grillakis et al., 2016; Li, Pontoppidan, et al., 2020; Nikolopoulos et al., 2011; Schröter et al., 2014; Sharma et al., 2018; Uber et al., 2018). Its effect on flood response varies with precipitation magnitude. For instance, initial soil moisture is believed to be more important during medium and smaller events than during extreme events of high-return period (Castillo et al., 2003; Grillakis et al., 2016; Wood et al., 1990).

Given the control of soil moisture and precipitation on flood response, soil moisture initialization and precipitation forecast are particularly important in flood modelling and forecasting (Berthet et al., 2009; Massari, Brocca, Barbetta, et al., 2014; Massari, Brocca, Moramarco, et al., 2014; Noto et al., 2008). On one hand, detailed in situ soil moisture observations are usually not available. Remote sensing soil moisture products, such as the advanced scatterometer (ASCAT, Bartalis et al., 2007) and the Soil Moisture Active Passive (SMAP, Entekhabi et al., 2010), although being widely used as an alternative of in situ observations to estimate soil moisture at regional and global scales (e.g., Abbaszadeh et al., 2020; Brocca et al., 2017; Massari, Brocca, Barbetta, et al., 2014), can only provide surface (the top several centimetres of the soil column) soil moisture information (Peng et al., 2017). On the other hand, uncertainties in initial soil moisture can propagate from the beginning of the modelling chain to the final streamflow simulation (Edouard et al., 2018; Silvestro & Rebora, 2014). To reduce such uncertainty, spin-up is usually adopted prior to a formal simulation. The purpose of spin-up is to let the model reach an equilibrium state at which the final results are subject to minimal influence from initial conditions (Ajami et al., 2014, 2015; Cosgrove et al., 2003; Seck et al., 2015). Different criteria (Ajami et al., 2014, 2015; Cai et al., 2014; Chen et al., 1997; Cosgrove et al., 2003; Yang et al., 1995) have been proposed and applied to define the equilibrium state following the guideline that model's states from two recursive runs are nearly identical. Thus, for flood forecast using a hydrometeorological model, one important task is to identify the time needed for the model to reach the equilibrium state. In addition, it is well acknowledged that the quantitative precipitation forecast is the major source of uncertainty in flood modelling using a hydrometeorological modeling system (Edouard et al., 2018; Vincendon et al., 2011; Wu et al., 2020). One commonly applied approach to quantify such

uncertainty is through convection-permitting precipitation ensemble simulation (e.g., Hsiao et al., 2013; Liu et al., 2017; Mackey & Krishnamurti, 2001; Nester et al., 2012; Wood & Lettenmaier, 2008). However, how uncertainties in precipitation forecast may propagate through the modelling chain remains an open question.

The objective of this study is to assess the impact of the initial soil moisture condition and precipitation magnitude on flood modelling using a hydrometeorological modelling chain. In this study, precipitation magnitude refers to the storm total rainfall during the event. And we use peak streamflow to characterize the flood because measurements are available at U.S. Geological Survey (USGS) stream gages (U.S. Geological Survey, 2022). We applied the Weather Research and Forecasting Model Hydrological modelling extension package (WRF-Hydro, Gochis et al., 2020) in both 'offline' and 'one-way coupled' mode to the Cape Fear River basin to simulate Hurricane Florence (Florence) induced flood in September 2018. Three research questions are investigated: (1) the influence of initial soil moisture on flood response and its connection with precipitation magnitude, (2) model spin-up behaviour and the associated flood modelling uncertainties, and (3) model uncertainty related to precipitation forecast ensembles and its sensitivity to model spin-up. The rest of the article is organized as follows. Section 2 describes material and methods, including study area information, model framework, and experiment design. Section 3 presents and discusses the model results. In Section 4, we close the article with a summary and conclusions. Our study is one of the very few applications of WRF-Hydro to simulate hourly streamflow over coastal river basins during hurricane-induced floods. The information derived from this study is essential in understanding the hydrometeorological and hydrological control of hurricane-induced floods, which will provide baseline knowledge for forecasting hurricane-induced flood using a hydrometeorological system.

## 2 | MATERIAL AND METHODS

### 2.1 | Study area and event

The Cape Fear River basin is located in the east-central North Carolina, United States (Figure 1a) and has a drainage area of 23 889 km<sup>2</sup>. From the headwater area to its coastal region, the elevation drops from 364 m to nearly 0 m (Figure 1b). The climate of Cape Fear River basin is subtropical with long, hot, humid summers and short, cold to mild winters. During 2002–2012, the average annual precipitation was ~1200 mm (Hamel & Guswa, 2015).

In this study, we focus our analysis on three major subbasins within the Cape Fear River basin (Figure 1b)-the Haw River subbasin above Bynum (USGS no. 02096960) in the upper part, Little River subbasin above Manchester (USGS no. 02103000) in the middle, and Black River subbasin above Tomahawk (USGS no. 02106500) over the lower basin. The Haw River subbasin is the largest and steepest of the three with a drainage area of 3302 km<sup>2</sup> and an average slope of 1.98° (Figure 1c). According to the 21 Category Modified International Geosphere-Biosphere Programme (IGBP) Moderate Resolution Imaging Spectrometer (MODIS) land cover product and the State Soil

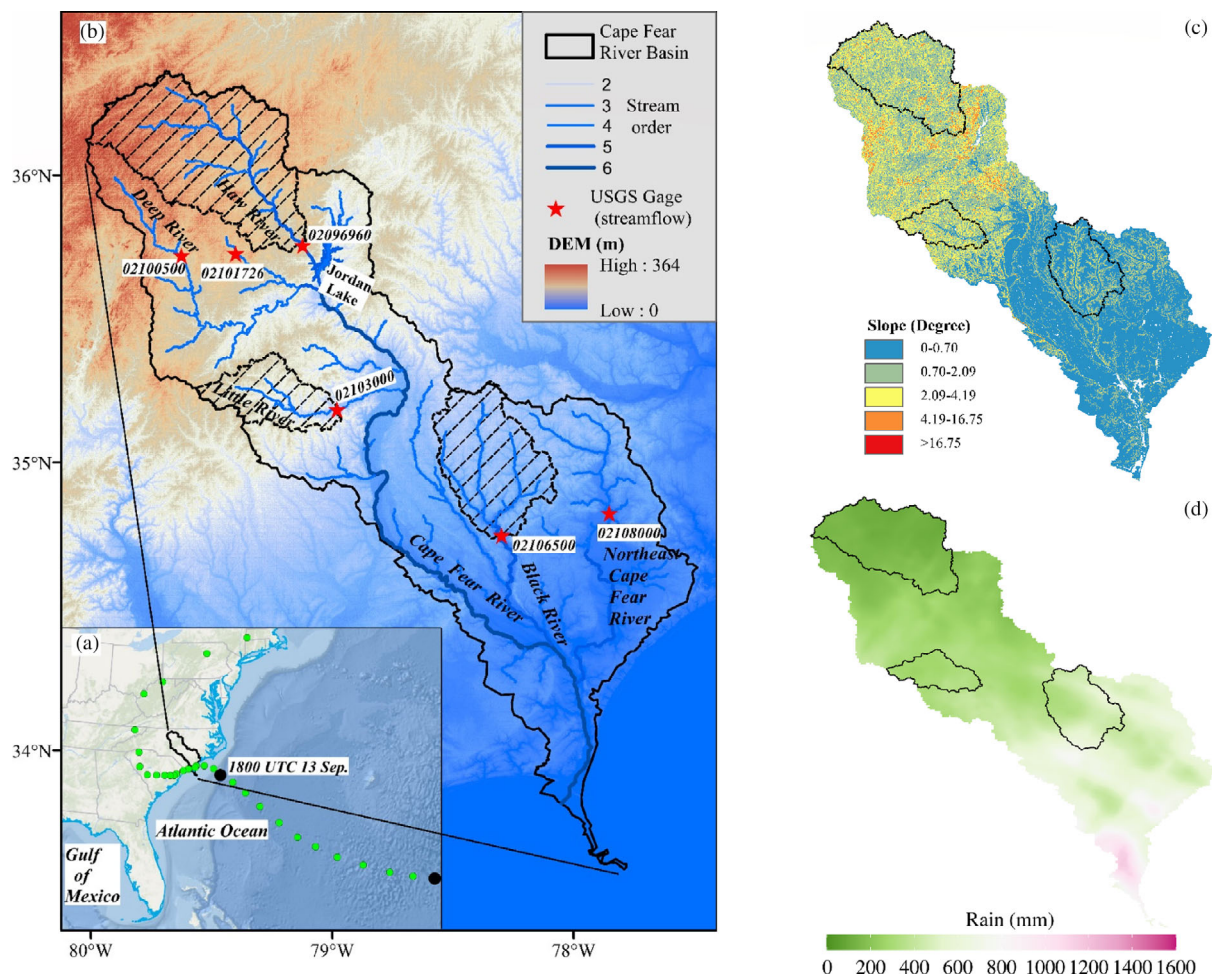


**FIGURE 1** (a) NOAA (National Oceanic and Atmospheric Administration of America) best track for hurricane Florence with 6 h interval. The cape fear river basin is outlined with solid black line. (b) Topography and river network in WRF-hydro domain (WHD01). The Haw River basin, Little River basin and Black River basin are filled with dashed lines. The USGS stream gages used are labelled with red stars. (c) Topographic slope in degree and (d) storm total rainfall during 0000 UTC 14 to 0000 UTC 18 September based on stage IV product across the cape fear river basin. The Haw River basin, Little River basin and Black River basin are outlined with solid black lines

Geographic Database (Miller & White, 1998), the soil and land cover in this subbasin are dominated by sandy loam (52%) and forest (44%), respectively. The Little River subbasin drains an area of 901 km<sup>2</sup> with an average slope of 1.92° (Figure 1c). Forest (66%) is the dominating land cover while the soil there is solely loamy sand. In sharp contrast, the topography in the Black River subbasin is much flatter and has an average slope of 0.67° (Figure 1c). It has a drainage area of 1751 km<sup>2</sup>. The land cover is mainly cropland/natural vegetation mosaic (57%), and the major soil type is loamy sand (53%).

In 2018, Florence swamped the Cape Fear River basin as the ninth-most-destructive hurricane ever hit the United States (Stewart & Berg, 2019). During its slow crest around the basin during the period of 14–18 September, it brought historic amounts of rainfall. According to Kunkel and Champion (2019), Florence ranked as the seventh largest rainfall event with a duration of 4 days for an area of 50 000 km<sup>2</sup>. Following the torrential rainfall, severe and widespread flooding occurred across the basin. The USGS stream gages at Little River at Manchester (USGS no. 02103000, Figure 1b), Black River near Tomahawk (USGS no. 02106500, Figure 1b) and Northeast Cape Fear

River near Chinquapin (USGS no. 02108000, Figure 1b) all observed peak streamflow with a ≥ 500-year return period (Feaster et al., 2018).

## 2.2 | The hydrometeorological modelling system

In this study, we selected WRF-Hydro (Gochis et al., 2020) due to its application flexibility in both ‘offline’ and ‘one-way coupled’ mode. In the ‘offline’ mode, WRF-Hydro can be driven by prescribed meteorological forcing such as the Phase 2 of the North American Land Data Assimilation System (NLDAS2) (Mitchell et al., 2004; Xia et al., 2012). While in “one-way coupled” mode, WRF-Hydro can be driven by outputs from an atmospheric model such as WRF (UCAR, 2019). Both offline (e.g., Somos-Valenzuela & Palmer, 2018; Xue et al., 2018; Yin et al., 2020, 2021) and one-way coupled (e.g., Kerandi et al., 2018; Li et al., 2017; Senatore, Davolio, et al., 2020; Senatore, Furnari, & Mendicino, 2020) WRF-Hydro have been successfully applied in hydroclimatic change, flooding and water budget studies. In operation, WRF-Hydro serves as the core component of the National Oceanic

and Atmospheric Administration National Water Model (NOAA NWM) in the United States, and of the Operational Flood Forecasting system operated by Israeli Hydrological Service in Israel.

As the first step of our study, WRF-Hydro was calibrated and evaluated in the offline mode and was driven by precipitation regridded from the Stage IV multi-sensor quantitative precipitation estimation product (Stage IV, Lin, 2011). Based on the multi-sensor hourly/6-hourly ‘Stage III’ analyses that were produced by the 12 River Forecast Centers (RFC) in CONUS on local 4 km polar-stereographic grids, Stage IV is mosaiced by the National Centers for Environmental Prediction (NCEP) as a national product (Lin, 2011). As a multi-sensor precipitation product, Stage IV ingests data from spatially complete and high-resolution radar as well as rain gauge networks. Other forcing variables including air temperature, wind, short and long wave radiation, humidity, and pressure were from NLDAS2. Once calibrated, a series of numerical experiments were carried out to investigate the first and second research questions as mentioned in Section 1. Following that, we applied WRF-Hydro in a one-way coupled mode with WRF to investigate the third research question.

### 2.2.1 | WRF-hydro: Setup, calibration and evaluation

As the hydrological component, WRF-Hydro V5.1.1 (Gochis et al., 2020) was used in this study. Built upon the Noah land surface

model with multi-parameterization options (Noah-MP, Niu et al., 2011), WRF-Hydro enhances the physical realism of the water cycle by integrating subsurface and overland flow routing, base flow and channel routing via the corresponding modules. In our study, subsurface routing, one-way overland routing, the bucket base flow model and diffusive wave routing are all activated. The computational domain of WRF-Hydro (WHD01) has a dimension of 2490 (west to east)  $\times$  3490 (north to south) with a horizontal grid spacing of 100 m (Figure 1b, Figure 2). The timestep of Noah-MP is set to 1 h while that of overland and channel routing in the hydrological simulation is 10 s.

WRF-Hydro was calibrated at Haw River near Bynum (USGS no. 02096960, Figure 1b), Little River at Manchester (USGS no. 02103000, Figure 1b) and Black River at Tomahawk (USGS no. 02106500, Figure 1b). The calibration period was from 0000 UTC 14–30 September 2018. We selected parameters controlling infiltration (refkdt), groundwater recharge (slope), saturated hydraulic conductivity (LKSATFAC), and overland and channel roughness (OVROUGHRTFAC and Mann) for calibration. The Haw River subbasin was calibrated automatically with NCAR’s WRF-Hydro calibration tool. The tool makes use of dynamically dimensioned search (DDS) methodology, which is designed for multiple parameters calibration and is ideally suited for a fully distributed model such as WRF-Hydro (Tolson & Shoemaker, 2007). For the Little River and Black River subbasins, we calibrated WRF-Hydro manually through a stepwise way following Yucel et al. (2015).

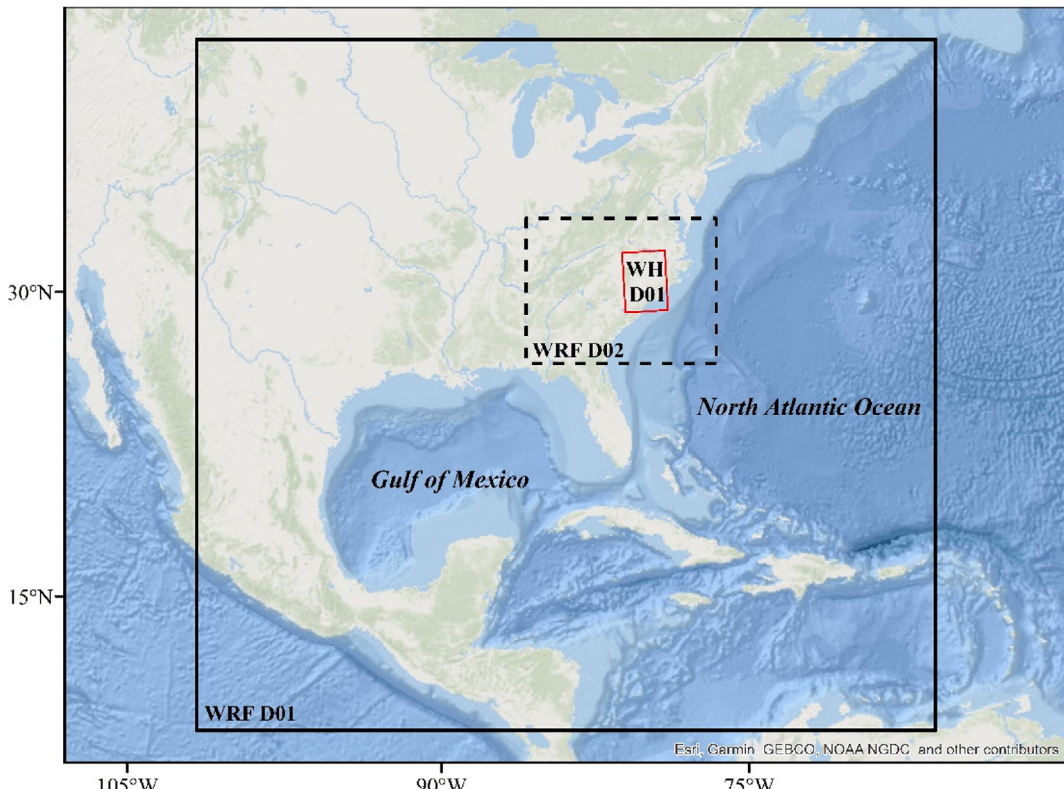


**FIGURE 2** Model domains: The outer domain of WRF (WRF D01, solid black line), the inner domain of WRF (WRF D02, dashed black line) and the domain of WRF-hydro (WH D01, solid red line).

Following the calibration, model evaluation was conducted. For Haw River subbasin, the model was evaluated at two stream gages in the neighbouring Deep River subbasin (USGS no. 02100500 and 02101726, Figure 1b) considering their similarity in land surface characteristics. Similarly for the Black River subbasin, parameter evaluation was conducted at a stream gage along the Northeast Cape Fear River (USGS no. 02108000, Figure 1b). For the Little River subbasin, as there is no independent stream gage to evaluate the calibrated parameters during Hurricane Florence, we carried out the evaluation over the same stream gage during another hurricane event-Hurricane Matthew (2016, Matthew hereafter). Formed as a category 5 hurricane at 0000 UTC 1 October 2016, Matthew made landfall around 1500 UTC 8 October along the central coast of South Carolina as a category 1 hurricane (Figure S1, Stewart, 2017). Three hours later after its landfall, the centre of Matthew moved back to the ocean and kept offshore of coastal North Carolina through 9 October 2016. During the 2 days it passed by the Carolinas, a large amount of rainfall was dumped over the study area. The maximum storm total rainfall recorded was 431 mm (Figure S1).

In addition to streamflow, we evaluated the simulated evapotranspiration (ET hereafter) against the remotely sensed 8-day ET from the MOD16 A2 Version 6 Evapotranspiration/Latent Flux product at 500-m resolution (MODIS ET hereafter, Running et al., n.d.; Mu et al., 2011) following previous studies (e.g., Lin, Rajib, et al., 2018; Parajuli et al., 2018; Xue et al., 2018).

To evaluate model performance, Nash-Sutcliffe coefficient (NSE, Equation [1]) was calculated in this study.

$$NSE = 1 - \frac{\sum_{t=1}^T (O_t - P_t)^2}{\sum_{t=1}^T (O_t - \bar{O}_t)^2}, \quad (1)$$

where  $O_t$  is the measured streamflow at time  $t$ ,  $P_t$  is simulated streamflow at time  $t$ ,  $\bar{O}_t$  is the mean of measured streamflow, and  $T$  is the total number of observations. Following Lin, Hopper, et al. (2018), a

NSE value of >0.4 is considered as satisfactory for hourly streamflow simulation under heavy rainfall events.

## 2.2.2 | WRF: Setup, configuration and ensemble design

WRF Version 4.0.1 (UCAR, 2019) was used to generate precipitation forecast ensembles. A one-way nested domain was built with a grid space ratio of 3 (Figure 2). The outer domain (WRF D01) covers the eastern, middle, and southern United States as well as the Gulf of Mexico with a grid spacing of 9 km. The inner domain (WRF D02) includes North and South Carolina with a grid spacing of 3 km. The vertical levels were 40 for both domains. The Yonsei State University scheme (YSU, Hong et al., 2006), the RRTM Model for GCMs (RRTMG, Iacono et al., 2008), the revised MM5 Monin-Obukhov surface layer scheme and the unified Noah-MP land-surface model (Niu et al., 2011) were selected for both domains. Tiedtke scheme (Michael Tiedtke, 1989; Zhang et al., 2011) was only applied for the outer domain (WRF D01).

To quantify the uncertainty from the precipitation forecast, we carried an ensemble simulation with 12 members (OFF1 to OFF12; Table 1). The initial and boundary conditions were provided by the fifth generation European Centre for Medium-Range Weather Forecasts (ECMWF) atmospheric reanalysis of the global climate (ERA5, Hersbach et al., 2020) with hourly interval and the final operational global analysis data from NCEP with a six-hour interval (NCEP-FNL, National Centers for Environmental Prediction/National Weather Service/NOAA/U.S. Department of Commerce, 2000). The horizontal resolution of ERA5 is 0.25° and that of NCEP-FNL is 1°. The WRF models were initialized at 1800 and 1200 UTC 13 September 2018, which is 18 and 24 h before landfall of Florence, respectively. Three microphysics schemes were applied, which are WRF Single-Moment 6-class (WSM6, Hong et al., 2005), Thompson graupel (Thompson hereafter, Thompson et al., 2008) and Morrison (Morrison hereafter,

**TABLE 1** Setup and configuration of WRF ensemble

Exp.	Initial and boundary condition	Microphysics scheme		Simulation period
		WRFD01	WRFD02	
OFF1	ERA5	WSM 6	Thompson	1800 UTC 13 September – 0600 UTC 18 September 2018
OFF2		Morrison		
OFF3		WSM 6	Thompson	
OFF4	NCEP-FNL	Morrison		
OFF5		WSM 6	Thompson	
OFF6		Morrison		
OFF7	ERA5	WSM 6	Thompson	1200 UTC 13 September – 0600 UTC 18 September 2018
OFF8		Morrison		
OFF9		WSM 6	Thompson	
OFF10	NCEP-FNL	Morrison		
OFF11		WSM 6	Thompson	
OFF12		Morrison		

Morrison et al., 2009). Microphysics refers to the sub-cloud-scale processes, which deals with the distribution and concentration of hydrometeor. Microphysics scheme is important to weather simulation because the formation, concentration and distribution of hydrometeor can highly influence the radiation, heat distribution and precipitation rate. The three microphysics schemes selected in this study belong to the bulk scheme, which apply a gamma distribution function to the concentration distribution of the specific type of hydrometeor. The detailed difference between these three schemes can be found in Bao et al. (2019). Hourly outputs from the inner domain (WRF D02) were regressed to the 1-km land surface model domain of the WRF-Hydro (WH D01) to provide forcing for the flood modelling.

### 2.3 | Experiment design

A total of 261 experiments was carried out to diagnose the influence of initial soil moisture on flood response and its connection with precipitation magnitude, model spin-up behaviour and the associated flood modelling uncertainties, as well as the uncertainty related to precipitation forecast (Table 2).

#### 2.3.1 | Soil moisture and precipitation magnitude (experiment suite E1)

To investigate the effect of initial soil moisture condition on flood response with respect to different precipitation magnitudes, we carried out WRF-Hydro offline simulations with eight initial soil moisture conditions combined with five precipitation magnitudes. The initial soil moisture condition varies from being 20%–90% saturated with a 10% interval. The precipitation magnitude was derived by multiplying the hourly rain rate from the Stage IV product with a factor of 0.6, 0.8, 1.0, 1.2 and 1.4, respectively. Here, we assume that the Stage IV is free of errors. In total, 40 experiments were conducted.

#### 2.3.2 | Spin-up behaviour and the associated uncertainties (experiment suite E2)

To assess the model's behaviour in response to spin-up time, we carried out another 17 experiments. In those experiments, the model was initialized from 1 to 17 months before the formal run at UTC 0000 14 September 2018, respectively. Streamflow, basin- and column-averaged soil moisture as well as basin-averaged latent heat flux was selected to evaluate the model's equilibrium state.

#### 2.3.3 | Precipitation induced uncertainty and its dependence on spin-up (experiment suite E3)

The precipitation outputs from 12 ensemble simulations (OFF1 to OFF12) described in Section 2.2.2 were used to drive WRF-Hydro to quantify the model uncertainty from precipitation forecast. We also investigated the variation of the model uncertainties from the precipitation forecast with different model spin-up time. For this, the 12 ensemble precipitation simulations were used to drive the hydrological model with 1–17 months spin-up described in Section 2.3.2.

## 3 | MODEL CALIBRATION AND EVALUATION

Table 3 details the model performance in simulating hourly streamflow and total ET. For streamflow, the NSE values at all stream gages during both calibration and evaluation events are all much higher than 0.4, indicating the satisfactory performance of WRF-Hydro in reproducing the flood response at a high-temporal resolution. It also suggests that a grid-based modelling system like WRF-Hydro is capable of providing flood forecast with reasonable accuracy at subbasin scales over a large coastal river basin with reliable forcing input, and when the spatial heterogeneity of land surface characters is appropriately considered.

In addition, Table 3 compares the simulated basin averaged total ET during 14–30 September 2018 against MODIS. On one hand, the model slightly overestimated the ET in the Haw River subbasin (4%), and the Black River subbasin (2%) compared to MODIS. On the other hand, in comparison to MODIS, our model underestimated the ET over the Deep River subbasin, the Little River subbasin, and the Northeast Cape Fear River subbasin by 11%, 12.7% and 3%, respectively. The correlation coefficient between modelled and MODIS ET is 0.59, which is in line with previous works (Bowman et al., 2015; Parajuli et al., 2018), implying a reliable model performance.

## 4 | RESULTS AND DISCUSSION

### 4.1 | Impact of initial soil moisture and precipitation magnitude on flood peak

Figure 3 shows the simulated relative flood peaks, which is defined here as the ratio between the simulated flood peak and the observed one, over the three subbasins with different initial soil moisture conditions and different precipitation magnitudes. The flood peaks generally increase with the initial soil moisture. Consistent with previous

**TABLE 2** Setup of the numerical experiments (N is the total number of simulations for each experiment suite)

Exp.	Model spin-up (month)	Initial soil moisture (% saturation)	Precipitation source	Precipitation Magnitude (multiplier)	N
E1	-	20, 30, ..., 90	Stage IV	0.6, 0.8, 1.0, 1.2, 1.4	40
E2	1, 2, ..., 17	-	Stage IV	-	17
E3	1, 2, ..., 17	-	WRF ensemble	-	204

**TABLE 3** Overview of WRF-hydro performance in modelling hourly streamflow and total evapotranspiration (ET)

River basin	NSE (hourly streamflow)			Total ET (mm)	
	Calibration	Evaluation independent stream gage	Evaluation independent event	Model	MODIS
Haw river	0.91	0.86 (USGS no. 02101726) 0.93 (USGS no. 02100500)	-	48.3	46.3
Little river	0.80	-	0.69	50.1	57.4
Black river	0.98	0.79	-	50.3	49.3
Deep river	-	-	-	51.4	57.1
Northeast Cape Fear river	-	-	-	49.9	51.3

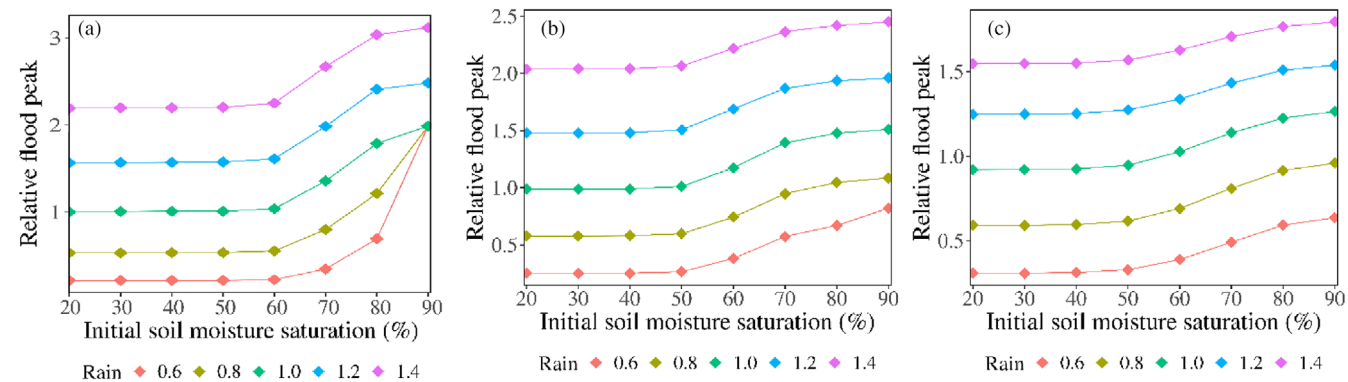


**FIGURE 3** Simulated relative flood peaks (dividing by observed) with different initial soil moisture conditions (%), the relative saturation) and different precipitation magnitudes over (a) Haw River basin at Bynum (USGS no. 02096960), (b) Little River basin at Manchester (USGS no. 02103000), and (c) Black River basin at tomahawk (USGS no. 02106500). Precipitation magnitude is normalized by that of the stage IV product. The locations of the stream gages and basins are shown in Figure 1b

studies (Grillakis et al., 2016; Silvestro & Rebora, 2014; Uber et al., 2018), we found that the impact of initial soil moisture on flood peak is non-linear. There exists a threshold value of the initial soil moisture, below which the sensitivity of flood peak to initial soil moisture is very low. As the soil moisture gets above the threshold value, the flood peak increases much more rapidly. This non-linearity is attributable to the crucial influence of soil moisture on the rainfall-runoff process (Zehe & Sivapalan, 2009). With low-soil moisture condition, water storage capacity is high and considerable amount of initial loss of rainfall to subsurface storage compartment can be expected. Similarly, with more saturated soil, precipitation magnitude will dominate the rainfall-runoff process and most of the rainfall is expected to become surface runoff. This results in rapid increase of flood peak once the initial soil moisture is higher than the threshold value. Due to this non-linear effect, flood peak from wet soil condition can be substantially larger than that when soil is drier. For instance, the simulated flood peak with 90% saturated initial soil moisture is almost two times of that with drier soil (less than 50% saturated, Figure 3).

This threshold effect underscores the pivotal role initial soil moisture, which is related to the soil properties, plays in modulating flood peaks. Grillakis et al. (2016) claimed that soil type can largely influence the threshold by controlling the hydraulic conductivity. Sandy soil is reported to be the main reason for the

threshold behaviour because of its high permeability (Komma et al., 2007, 2008). On the other hand, the relationship of flood peak and initial soil moisture tends to be more linear over areas with shallow and more impermeable soils (Grillakis et al., 2016). In addition, the threshold can be increased with the presence of preferential pathways such as opening cracks or root channels in the soil (Vogel, Hoffmann, Leopold, et al., 2005; Vogel, Hoffmann, & Roth, 2005; Zehe & Sivapalan, 2009). For the case of our study, it can be observed that the threshold value in the Haw River subbasin (~60%) is higher than that in the Little River and the Black River subbasins (~50%, Figure 3), likely because the soil type in the Haw River subbasin is dominated by sandy loam while the other two subbasins are mainly loamy sand.

Previous studies reported largely varied threshold values. A threshold of 34% saturation was found by Uber et al. (2018) over the Cévennes–Vivarais region in southern France. Penna et al. (2011) observed a value of 45% saturation in a small headwater catchment in the Italian Alps. Mcmillan et al. (2014) tested the threshold behaviour of soil moisture on event runoff based on observations over a mid-sized catchment in Northland, New Zealand. They found that the threshold values can range from 27% saturation to 58% saturation. Moreover, a threshold value of 50% saturation was reported by Grillakis et al. (2016) over two catchments in Crete and Austria. Further, a threshold soil moisture that approximates 80% saturation was

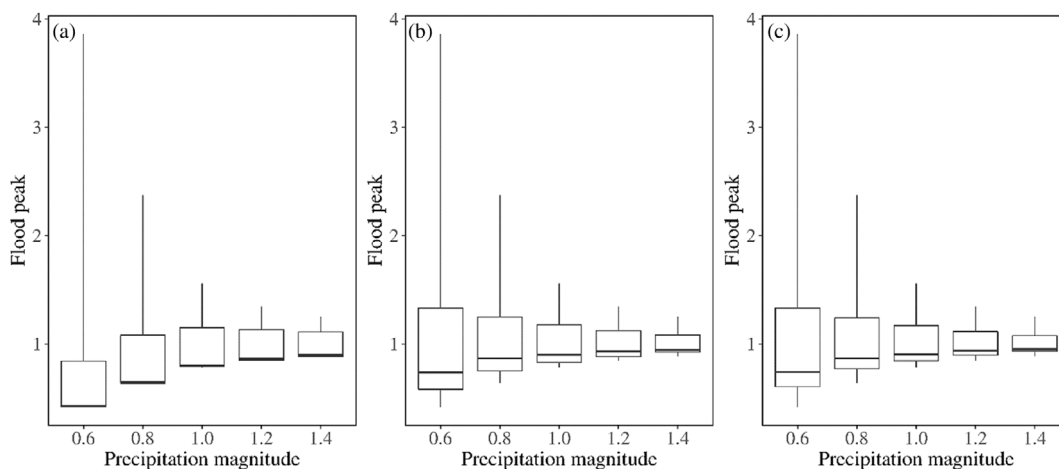


**FIGURE 4** Boxplots of the normalized flood peaks (dividing by the mean) from various initial soil moisture conditions for different precipitation magnitudes over (a) Haw River basin at Bynum (USGS no. 02096960), (b) Little River basin at Manchester (USGS no. 02103000), and (c) Black River basin at tomahawk (USGS no. 02106500). Precipitation magnitude is normalized by that of the stage IV product. The locations of the stream gages and basins are shown in Figure 1b. Boxplots show the minimum value, first (lower) quartile, median, third (upper) quartile, and maximum value

observed for runoff generation in southwestern Wisconsin agricultural watersheds (Radatz et al., 2013).

We also investigated how the influence of initial soil moisture on flood peak vary with the precipitation magnitude. Figure 4 shows the normalized flood peaks (dividing by the mean) under different precipitation magnitudes with eight different initial soil moisture conditions. In the three subbasins, flood peak variation decreases as precipitation magnitude increases. In line with previous studies (Castillo et al., 2003; Grillakis et al., 2016; Nikolopoulos et al., 2011; Noto et al., 2008; Silvestro & Rebora, 2014; Wood et al., 1990), this trend indicates that the role initial soil moisture plays in modulating flood response weakens as precipitation magnitude increases. It is because that the soil's holding capacity can be easily filled at the beginning of the heavy rainfall event. Then the runoff generation is controlled by precipitation instead of initial soil moisture. For our study area, we can take Florence induced precipitation as a benchmark value. For hurricanes with precipitation magnitude smaller than Florence, initial soil moisture condition has the potential to exert an important influence on flood peak. Whereas, for events with precipitation magnitude bigger than that of Florence, initial soil moisture condition seems to have limited influence on flood peak (Figure 4). Thus, in light of the projected precipitation increase associated with Atlantic hurricanes (Knutson et al., 2010), as well as the unprecedentedly high precipitation since the late 1990s (Paerl et al., 2019), better understanding of rainfall characteristics (especially precipitation magnitude) seems to be more important than initial soil moisture conditions in flood forecasting associated with extreme events. Take Hurricane Harvey as an example, for an area sized 50 000 km<sup>2</sup>, Harvey is the single largest rainfall event with a duration of 4 days (Kunkel & Champion, 2019). According to Li, Zhao, et al. (2020), the antecedent rainfall event only plays a minor role in the floods at Houston reservoirs associated with Harvey. Whereas, a redistribution of the rainfall field due to the

change of Harvey's track could have induced a significantly larger (49%) total volumetric flow than was actually measured (Li, Zhao, et al., 2020).

## 4.2 | Spin-up behaviour and associated model uncertainties

### 4.2.1 | Spin-up behaviour

In this study, following Seck et al. (2015) and Ajami et al. (2014), we define three different criterion of equilibrium state at which the relative difference of model variables in recursive runs are less than 10% ('practical' equilibrium), 1% and 0.1% (final equilibrium), respectively. We selected channel averaged streamflow (SF), basin and column averaged soil moisture (SM) and basin averaged latent heat flux (LH) as the prognostic variables to quantify equilibrium conditions. Based on the model results from the 17 spin-up experiments (E2, Table 2), we calculated the percent change of model states at 0000 UTC 14 September 2018 among these recursive runs.

Calculated percent change of the selected variables with spin-up time and the number of months needed for the model to reach equilibrium are shown in Table 4 and Figure 5. In general, the model reaches the 'practical' equilibrium (<10%) for all three variables in the three subbasins with less than 4 months of spin-up (Table 4). Before that, large variation exists between recursive experiments (Figure 5a–c) and decreases with spin-up time. This variation indicates the dominating influence of the most recent meteorological events on hydrologic state over older ones. Soil moisture dried up in the first and third month and increased during the second month prior to Florence. This led to the large positive and negative difference between simulations with two- and one-month spin-up, and simulations with

**TABLE 4** Number of months required for the model to reach equilibrium (LH: Basin averaged latent heat flux, SF: Channel averaged streamflow, SM: Basin and column averaged soil moisture. The percentages indicate the relative difference which model variables in recursive runs are less than)

River basin	10%			1%			0.1%		
	LH	SF	SM	LH	SF	SM	LH	SF	SM
Haw river	2	4	3	7	12	6	15	13	12
Little river	2	3	2	3	5	2	12	12	5
Black river	2	2	2	3	11	2	12	-	12

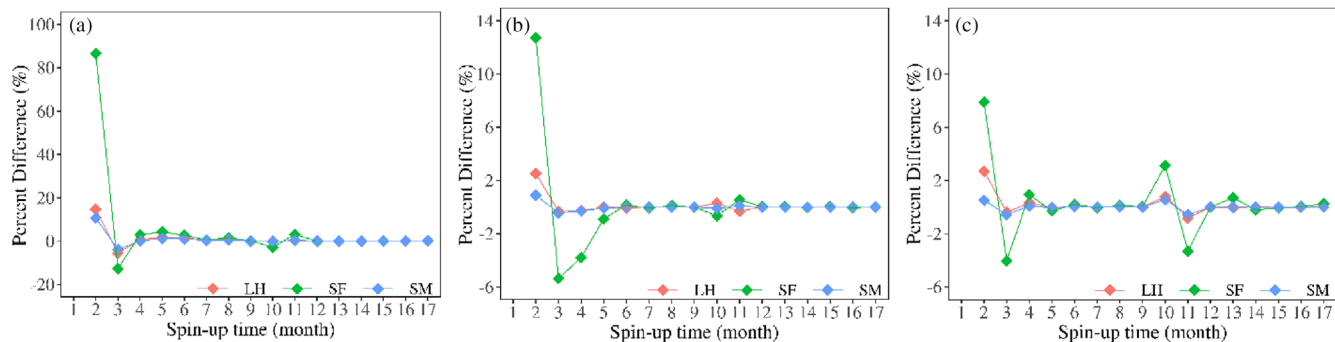


**FIGURE 5** Estimated percent change of basin averaged latent heat flux (LH, red), channel averaged streamflow (SF, green) and basin and column averaged soil moisture (SM, blue) at first hours of simulations (0000 UTC 14 September 2018) between recursive experiments for (a) Haw River basin above Bynum (USGS no. 02096960), (b) Little River basin above Manchester (USGS no. 02103000), (c) Black River basin above tomahawk (USGS no. 02106500). The locations of the basins and stream gages are shown in Figure 1b

three- and two-month spin-up, respectively. The latent heat flux shows similar pattern with spin-up time as soil moisture, which is due to the control of soil moisture on it (Gu et al., 2006). In addition, streamflow exhibits similar but much more pronounced variation. The maximum difference of streamflow among recursive experiments is  $\sim 87\%$ , which is found between simulations with one- and two-month spin-up (Figure 5a). This amplification is due to the non-linear control of soil moisture on runoff process as mentioned in Section 4.1. And it suggests the importance of soil moisture equilibrium in streamflow simulation as suggested by Ajami et al. (2014).

Once the ‘practical’ equilibrium is reached (Table 4), the percent difference gets stabilized and decreases rapidly (Figure 5a–c). Soil moisture and latent heat flux still exhibit similar behaviour with comparable time needed to reach the 1% equilibrium. However, it takes longer for streamflow to equilibrate at 1% than the other two variables. Moreover, for the final equilibrium ( $<0.1\%$ ), the three variables generally equilibrate with comparable spin-up time. It should be noted that the streamflow over the Black River subbasin did not reach final equilibrium after 17 months spin-up. However, the absolute difference between the last two recursive runs is only  $0.004 \text{ m}^3/\text{s}$ .

The three selected subbasins exhibit similar spin-up behaviour to reach ‘practical’ equilibrium. This indicates the dominating effect from the most recent meteorological conditions on hydrological state. However, the magnitude of percent difference between recursive runs over the Haw River subbasin (Figure 5a) is much larger (Figure 5b,c), and it in general takes longer to reach 1% and 0.01% equilibrium than the other two subbasins (Table 4). This can be explained by the difference in hydrologic system memory among the

three subbasins (Seck et al., 2015). Hydrologic system memory is positively related to the time between the basin’s current state and the earliest precipitation event responsible for it. The Haw River subbasin is characterized by much lower infiltration capacity but higher saturation conductivity. These properties exacerbated the dryness by depleting the soil moisture and by decreasing the infiltration. In this case subsurface deficit occurs and leads to longer hydrologic system memory (Seck et al., 2015).

#### 4.2.2 | Model uncertainties associated with spin-up

In this section we quantify model uncertainties related to spin-up. Here, the simulated flood peak with the 17-month spin-up is treated as the equilibrium condition. The percent bias of the simulated flood peaks from the equilibrium one over the three selected subbasins are shown in Figure 6 (blue). To illustrate the influence of spin-up on model uncertainty, the percent bias of basin and column averaged soil moisture (SM, red) for each subbasin at the first hour of simulations (0000 UTC 14 September 2018) with various spin-up time from equilibrium condition is also shown. For all the selected subbasins (Figure 6a–c), model bias of flood peaks exhibits a similar pattern with spin-up time following that of the initial soil moisture. Such similarity indicates the persistence and propagation of bias in initial condition through the modelling chain to the simulated flood peak. In addition, the higher magnitude of flood peak bias than that of the initial soil moisture implies the amplification of model uncertainty from initial soil moisture condition. This amplification is due to the threshold effect of soil moisture on flood peak as discussed in

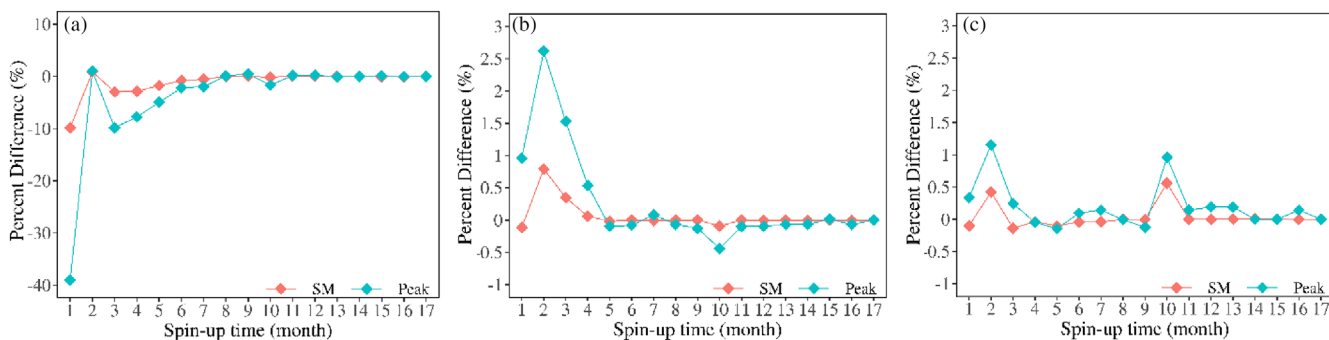


**FIGURE 6** The percent bias of the simulated flood peaks (peak, blue) with different spin-up time from the equilibrium over (a) Haw River basin at Bynum (USGS no. 02096960), (b) Little River basin at Manchester (USGS no. 02103000) and (c) Black River basin above tomahawk (USGS no. 02106500). The simulation with 17-month spin-up is assumed to be the equilibrium run. For comparison, the percent bias of basin and column averaged soil moisture (SM, red) for each basin at the first hour of simulations with various spin-up time (0000 UTC 14 September 2018) from equilibrium condition is also shown. The locations of the basins and stream gages are shown in Figure 1b

River basin	10% equilibrium <sup>a</sup>	1% equilibrium <sup>a</sup>	0.1% equilibrium <sup>a</sup>
Haw river	-9.82% (-143 m <sup>3</sup> /s)	-2.18% (32 m <sup>3</sup> /s)	0.24% (3 m <sup>3</sup> /s)
Little river	2.62% (13 m <sup>3</sup> /s)	2.62% (13 m <sup>3</sup> /s)	-0.10% (<1 m <sup>3</sup> /s)
Black river	1.16% (17 m <sup>3</sup> /s)	1.16% (17 m <sup>3</sup> /s)	0.19% (3 m <sup>3</sup> /s)

<sup>a</sup>The equilibrium states are determined based on basin and column averaged soil moisture as shown in Table 4.

Section 3.2. As the spin-up time increases, the bias of simulated flood peak decreases.

In Table 5, we listed the flood peak bias from simulations with different spin-up time corresponding to the three equilibrium conditions. For the three subbasins, once model state reaches 1% or 0.1% equilibrium, the bias of simulated flood peak is minimal. We noted that the flood peak bias at the Little River and Black River subbasins never exceeds 2.62% (13 m<sup>3</sup>/s, Table S1) and 1.16% (17 m<sup>3</sup>/s, Table S1), respectively, regardless of the spin-up time. However, large bias still exists at the Haw River subbasin even the model reaches ‘practical’ equilibrium. We attribute this difference to the influence of precipitation magnitude on the modulating effect of soil moisture on flood peak. During Florence, 269 and 411 mm rainfall fell over the Little River subbasin and the Black River subbasin, respectively, which is much larger than the 122 mm rainfall over the Haw River subbasin (Yin et al., 2021). In addition, according to our model results, the basin and column averaged initial soil moisture in the former two subbasins are 26.5% and 22.7%, respectively, which is much lower than that of the Haw River subbasin (29.6%). Thus, the combination of the high-soil moisture and low-precipitation magnitude in the Haw River subbasin led to its higher sensitivity to spin-up time, whereas initial soil moisture’s influence on flood peak in the Little River and the Black River subbasins is damped by the large precipitation magnitude.

To gain an insight of spatial distribution of spin-up induced uncertainty, we computed the percent bias of simulated flood peaks with 1-, 3- (10% equilibrium), 6- (1% equilibrium) and 12-month (0.1% equilibrium) spin-up from the equilibrium run over all channel elements (Figure 7). For reference, the simulated flood peaks from equilibrium

**TABLE 5** Simulated flood peak bias with spin-up at three different equilibrium states

run over all the channel elements is shown in Figure S2. The percent bias exhibits spatial variation in simulated flood peaks before model reaching ‘practical’ equilibrium (Figure 7a). Substantial underestimation is found in upper and coastal areas of the Cape Fear River basin while overestimation is found in the middle part of the basin. As the spin-up time increases, the spatial heterogeneity of the flood peak bias decreases. As the model reaches ‘practical’ equilibrium state with 3 months spin-up (Figure 7b), the flood peak bias over the lower and middle part of the basin become minimal while large overestimation still exists over the upper basin. Once the model reaches 1% (Figure 7c) or 0.1% equilibrium (Figure 7d), the simulated flood peaks over the whole channel network get close to the equilibrium state with bias only found over several small segments. The spatial heterogeneity of bias suggests different spin-up behaviour across the basin, which is attributable to the difference in hydrologic system memory. In this case, even for a fully distributed, multi-scale model like WRF-Hydro, inadequate spin-up can result in unreliable simulation of flood at different scales with either overestimation or underestimation depending on the local hydrologic system memory.

#### 4.3 | Ensemble precipitation simulation and associated modelling uncertainty

##### 4.3.1 | Ensemble precipitation simulation

Figure 8 shows the simulated precipitation magnitude over the Cape Fear River basin for the 12 WRF ensemble members. Their

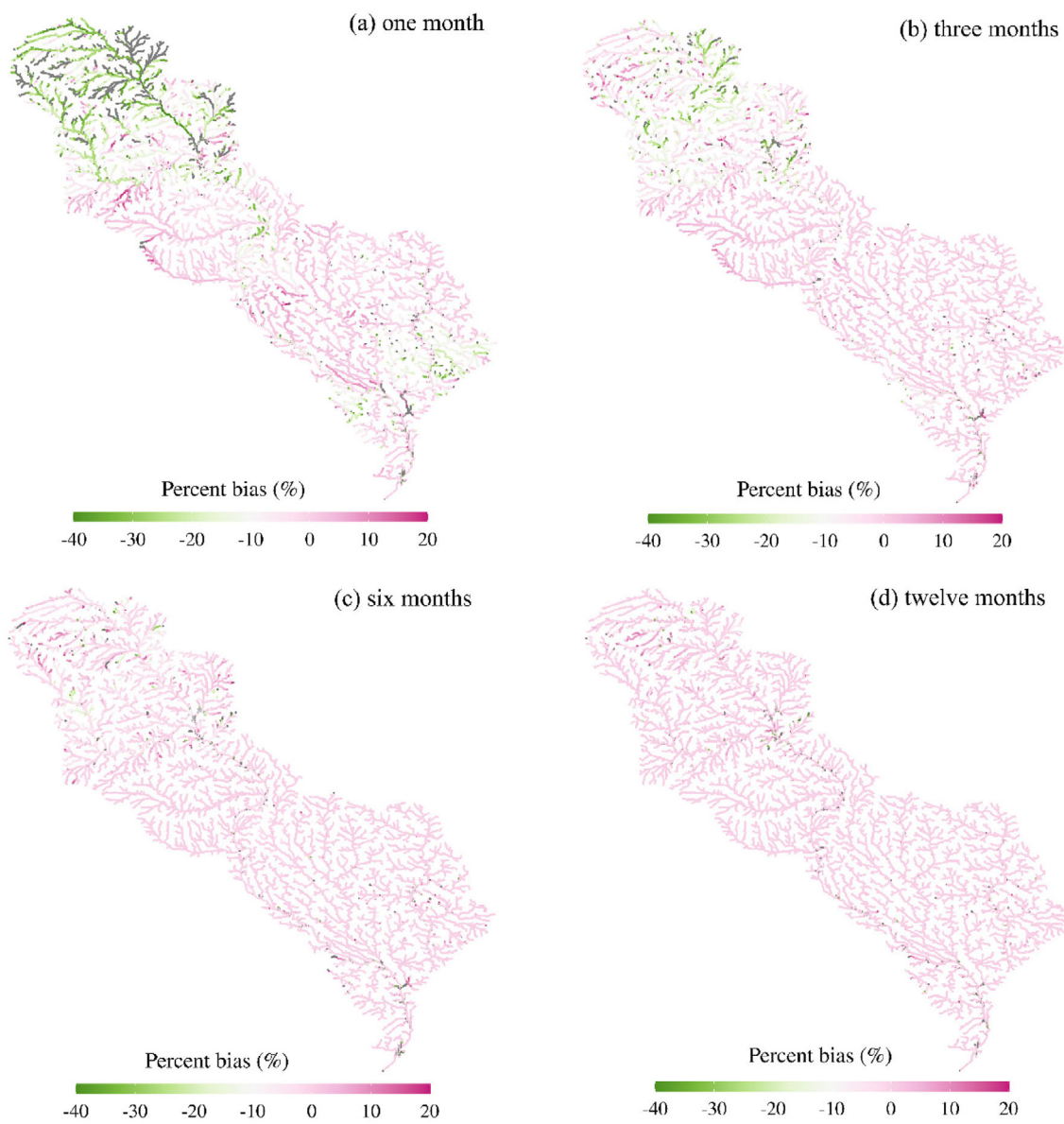


**FIGURE 7** The percent bias of the simulated flood peaks with spin-up of (a) 1 month, (b) 3 months (10% equilibrium), (c) 6 months (1% equilibrium) and (d) 12 months (0.1% equilibrium). The simulation with 17 months spin-up was assumed to be the equilibrium run. The channel network of the model is shown in Figure 1b

differences from the Stage IV product (simulation subtracted by Stage IV) are shown in Figure S3. The simulation can generally reproduce the spatial pattern of the precipitation magnitude with higher values over coastal areas and lower values in the upper part of the basin. For each ensemble member (Figure S3), both over- and under- estimation can be found across the whole basin. The simulations driven by NCEP-FNL (Table 1, Figure S3d-f,j-l) exhibit an overall overestimation pattern over the basin. While the simulations forced by ERA5 exhibit either overestimation-dominated (Figure S3a,g) or underestimation-dominated patterns (Figure S3b,c,h,i) depending on the microphysics scheme applied. For the three selected subbasins, the ensemble precipitation simulation in general result in overestimation compared to the Stage IV product.

Two (Figure S3b,c) and four (Figure S3b,c,h,i) out of 12 ensemble members exhibit underestimation in terms of precipitation magnitude in comparison to Stage IV over the Haw River subbasin and the Little River subbasin, respectively. While for the Black River subbasin, all ensemble members result in an overestimation. The overestimation of the convection-permitting models associated with high-precipitation intensities is a common problem that has been well documented by previous studies (Kendon et al., 2012; Pal et al., 2019; Woodhams et al., 2018).

Time series of basin-averaged hourly rain rate of the three subbasins from the ensemble precipitation simulations are compared against the stage IV product in Figure 9. Simulated hourly rain rate varies substantially among the ensemble members and the variation generally

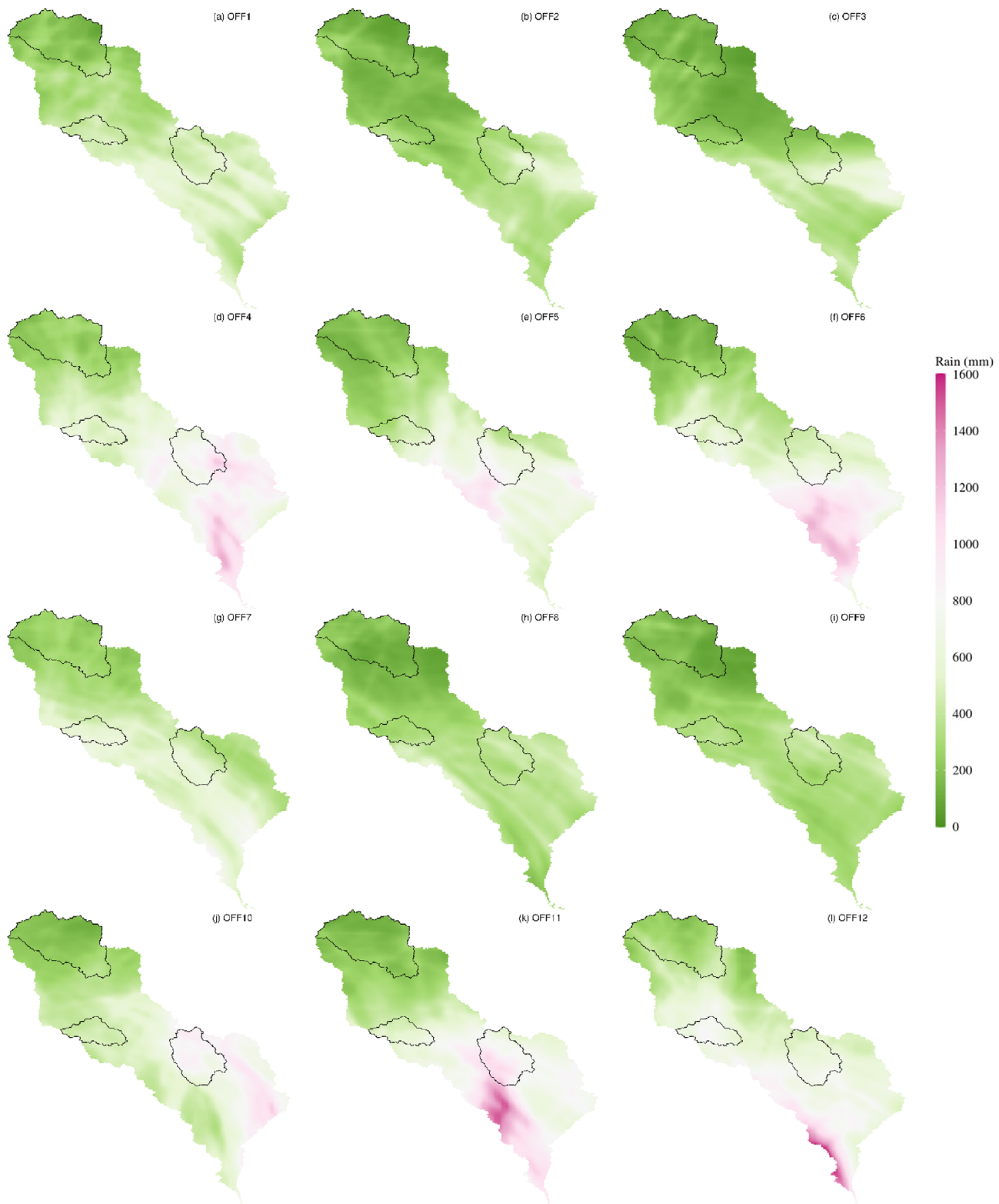
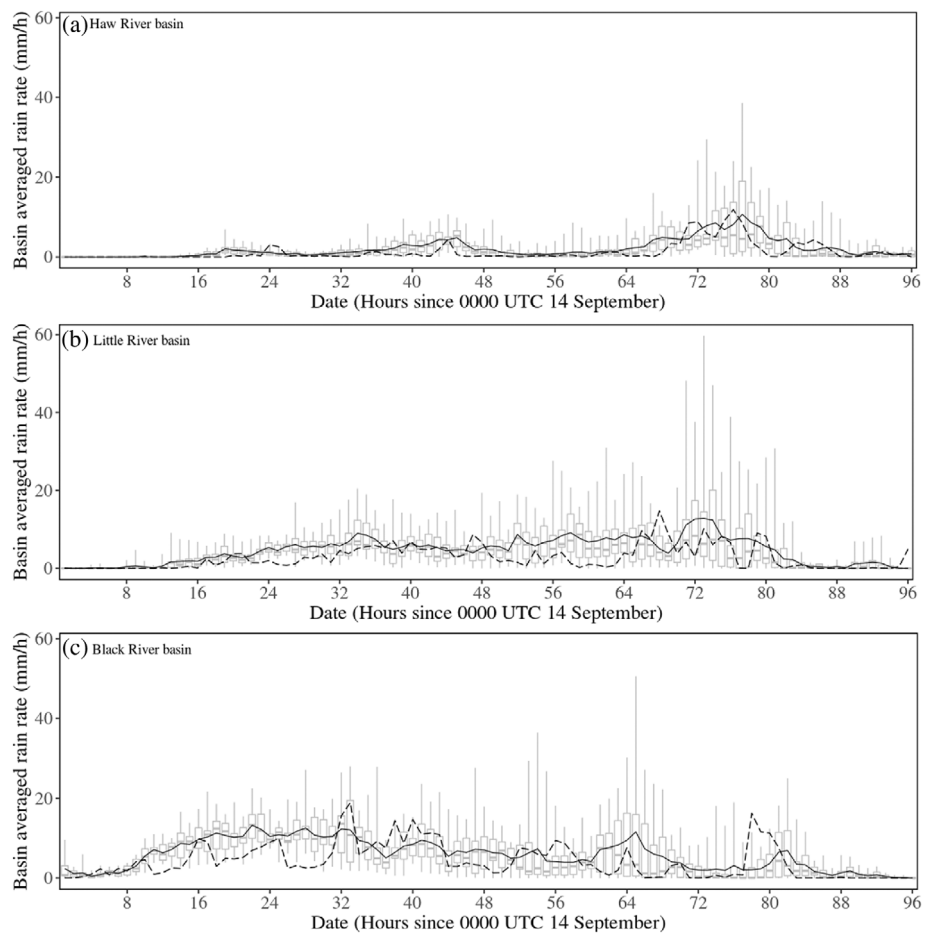


**FIGURE 8** Spatial distribution of the storm total rainfall during Florence (09/140000–09/180000 2018) over the cape fear river basin for the 12 ensemble members. The three selected basins are outlined with solid black lines

increases as the rain rate increases. The ensemble mean can generally capture the multi-peak signature of the rainfall time series, which is the result of the storm motion and rainband structure evolution. A

general overestimation of the ensemble mean in comparison to the stage IV product is observed during most of the simulation period and is more salient when rain rate is high.

**FIGURE 9** Time series of basin averaged hourly rain rate (mm/h) for (a) Haw River basin above Bynum (USGS no. 02096960), (b) Little River basin above Manchester (USGS no. 02103000), (c) Black River basin above tomahawk (USGS no. 02106500) from the 12 ensemble members with minimum, lower quartile, median, upper quartile, and maximum depicted by box plot from the simulation during 0000 UTC 14 to 0000 UTC 18 September. The ensemble mean is shown in black line while the stage IV rainfall is in dashed black line. The locations of the basins and stream gages are shown in Figure 1b. Boxplots show the minimum value, first (lower) quartile, median, third (upper) quartile and maximum value



#### 4.3.2 | Model uncertainty associated with precipitation forecast

We used the precipitation outputs from the 12 WRF ensemble simulations to drive the hydrological model (one-way coupled). Figure 10a–c evaluates the simulated flood hydrographs for the ensemble members and the ensemble mean against the streamflow simulated using stage IV product. Figure 10d exhibits the bias of simulated basin-averaged precipitation magnitude and associated flood peaks. Variations can be found over the simulated flood hydrographs among the ensemble members over all three subbasins. The percent bias at the outlets of the subbasin range from –29% to 480% in the Haw River subbasin, –51% to 562% in the Little River subbasin, –42% to 153% in the Black River subbasin. This large variation of the uncertainty related to precipitation forecast underscores the necessity of implementing an ensemble forecasting instead of the traditional deterministic forecast. In addition, the bias introduced by precipitation forecasts is larger than that introduced by model spin-up as discussed in Section 4.2, which emphasizes the dominant role of precipitation forecast in flood modelling uncertainties. Moreover, the flood peak bias is larger than the bias of precipitation magnitude in all three subbasins (Figure 10d). This indicates the amplification of precipitation forecast bias as it propagates through the modelling chain to the flood peak simulation. The amplification effect can be attributed to the

combined influence of the bias in the magnitude and spatial distribution of precipitation.

We then investigated the variation of precipitation forecast induced model uncertainty on model spin-up. As shown by the boxplots in Figure 11, a large degree of model uncertainty can be induced by precipitation forecast regardless of the spin-up time over all three selected subbasins. This emphasizes the dominating influence of precipitation forecast on flood modelling uncertainty over model initialization (Figure 10). The dominance of precipitation forecast is partly because heavy precipitation dampens the modulation by soil moisture over flood response as shown in Figure 4.

The effect of the spin-up time on flood modelling can be observed by the variation of the ensemble mean (Figure 11 and Figure 12) before the model reaches “practical” equilibrium with a 3-month spin-up. This implies the modulation of the initial soil moisture on the distribution of flood peaks from ensemble simulations, which is attributed to the relatively large variation of soil moisture state in the hydrological model prior to ‘practical’ equilibrium (Figure 6). However, the modulation effect becomes minimal once the hydrological model reaches the ‘practical’ equilibrium and the flood peak bias solely depends on the precipitation forecast. Moreover, it should be noted that once the model reaches the ‘practical’ equilibrium, the absolute change in percent bias (calculated from relative difference between recursive spin-up runs) of ensemble mean is less

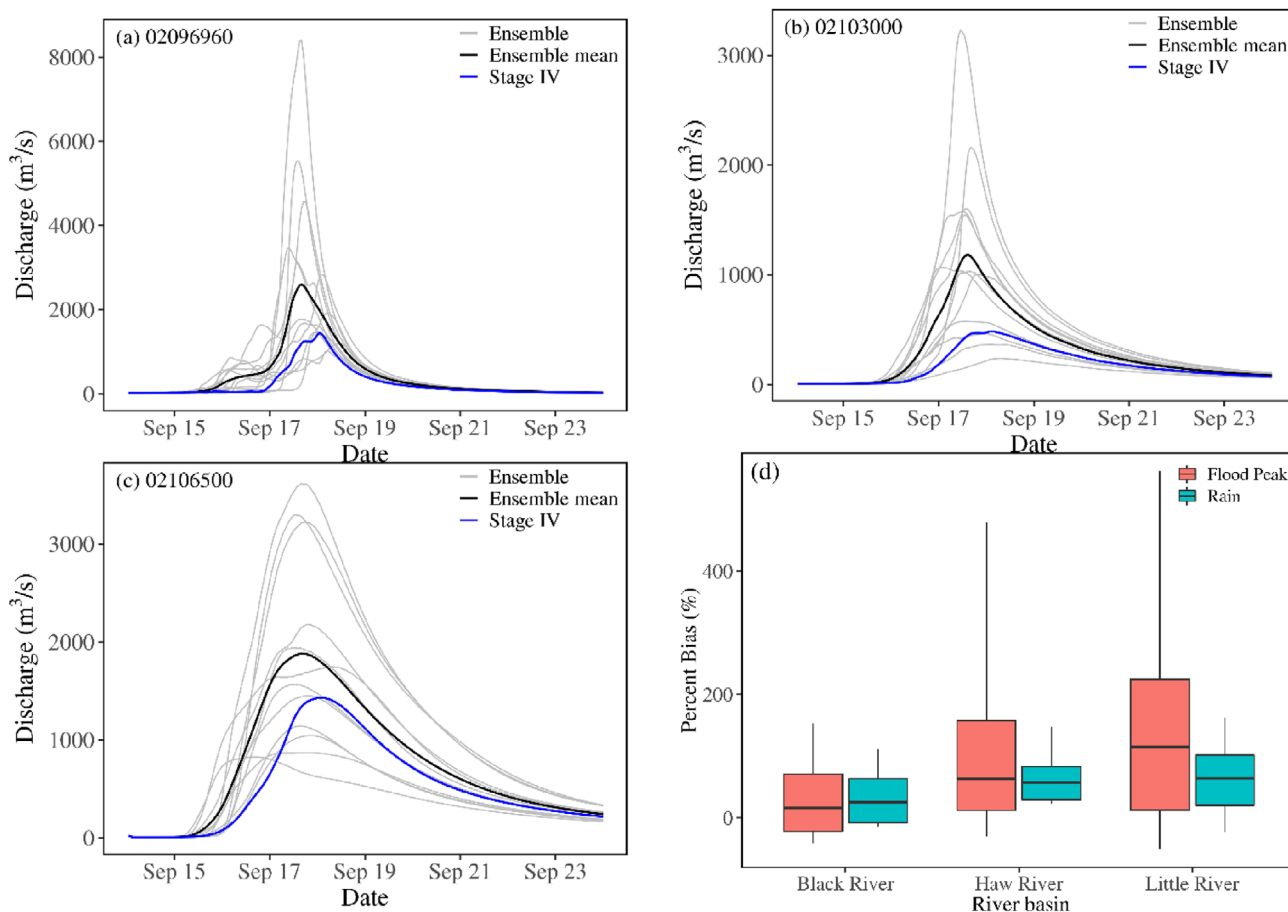


**FIGURE 10** The modelled flood hydrographs driven by 12 ensemble rainfall (grey line), the ensemble mean (black line), and by stage IV rainfall (blue line) over (a) Haw River basin at Bynum (USGS no. 02096960), (b) Little River basin above Manchester (USGS no. 02103000) and (c) Black River basin above Tomahawk (USGS no. 02106500). (d) Boxplots of the percent bias of simulated basin averaged rainfall relative to stage IV observations, and of simulated flood peaks driven by WRF ensemble simulations in comparison to that driven by stage IV product. The locations of the stream gages are shown in Figure 1b. Boxplots show the minimum value, first (lower) quartile, median, third (upper) quartile, and maximum value

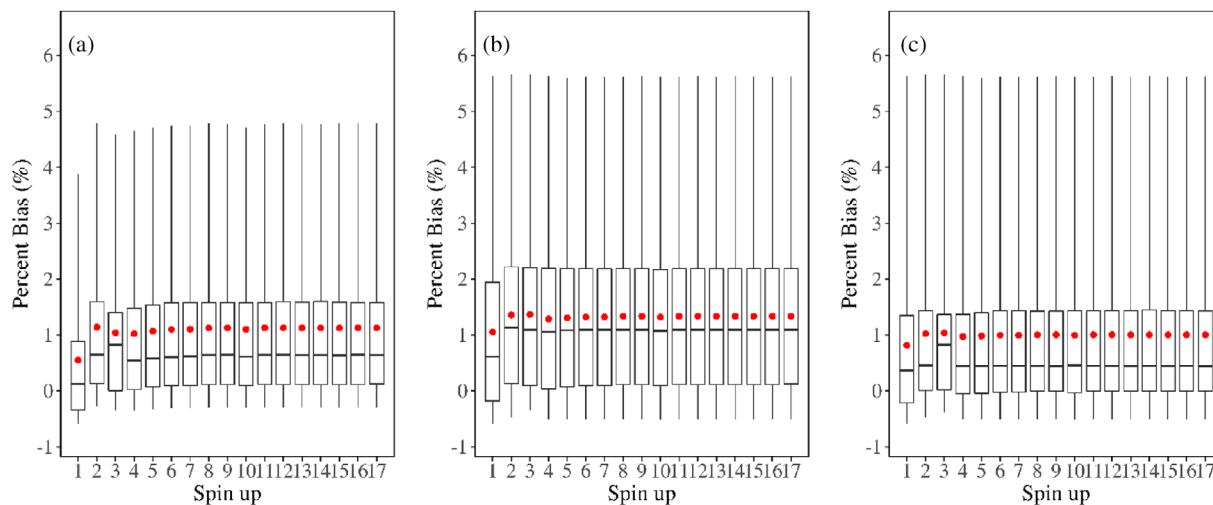


**FIGURE 11** Boxplots of the percent bias of simulated flood peak from 12 ensemble simulations relative to that from stage IV over (a) Haw River basin at Bynum (USGS no. 02096960), (b) Little River basin above Manchester (USGS no. 02103000) and (c) Black River basin above Tomahawk (USGS no. 02106500). The ensemble mean is shown in red dot. The locations of the stream gages are shown in Figure 1b. Boxplots show the minimum value, first (lower) quartile, median, third (upper) quartile and maximum value

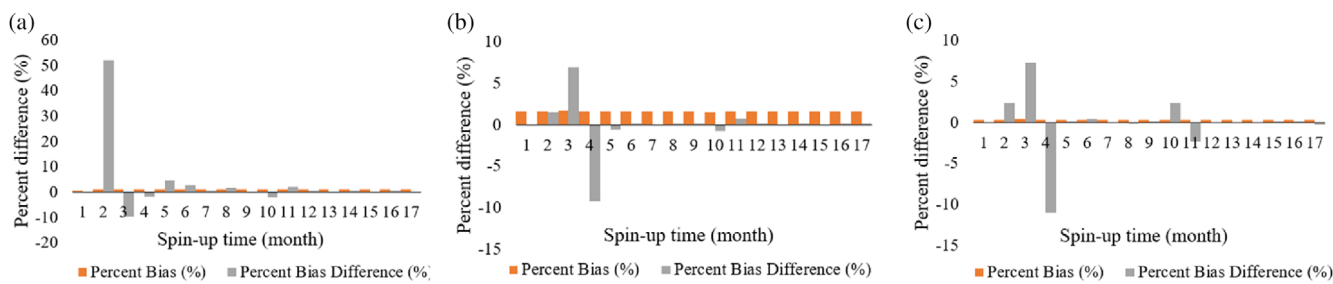


**FIGURE 12** The percent bias of the ensemble mean flood peak (dark orange) relative to that driven by stage IV product with different spin-up time and the change in percent bias (grey) between recursive spin-up runs over: (a) Haw River basin at Bynum (USGS no. 02096960), (b) Little River basin above Manchester (USGS no. 02103000) and (c) Black River basin above tomahawk (USGS no. 02106500). The locations of the stream gages are shown in Figure 1b

than 1% (Figure 12). This indicates that in flood forecasting practise, a ‘practical’ equilibrium spin-up should be adequate to minimize spin-up induced uncertainty.

## 5 | SUMMARY AND CONCLUSIONS

In this study we applied WRF-Hydro model in both ‘offline’ and ‘one-way coupled’ mode to investigate the effect of initial soil moisture and precipitation magnitude on flood response. In addition, we studied the model spin-up behaviour and the associated uncertainties in flood modelling throughout a hydrometeorological modelling chain. We also performed a precipitation ensemble simulation to understand the modelling uncertainty related to precipitation forecast and its dependence on spin-up. The major results from this study are summarized as follows:

1. For the control of initial soil moisture on flood peak, there is a threshold value with initial soil saturation being 50%–60%. Below the value, the flood peak shows little sensitivity to the initial soil moisture. Above the threshold value, the flood peak increases rapidly with initial soil moisture. In addition, the flood peak variation due to different initial soil moisture conditions decreases as the precipitation magnitude increases.

2. For the spin-up of WRF-Hydro, the model reaches “practical” equilibrium (10%) within 4 months and 1% equilibrium within 12 months regardless of the prognostic variables used. In general, the streamflow converges slower than soil moisture and latent heat flux.

3. Both the uncertainty from model spin-up and precipitation forecast can propagate through the hydrometeorological modelling chain and get amplified in the simulated flood peak. For the ensemble flood forecasting, the modelling uncertainty is dominated by the precipitation forecast and is modulated by model spin-up. Spin-up induced uncertainty is minimal once the model reaches ‘practical’ equilibrium.

Consistent with previous studies (Grillakis et al., 2016; Silvestro & Rebora, 2014; Uber et al., 2018), the results achieved here show that the initial soil moisture modulates the flood peak in a nonlinear way. The modulation effect gets damped as the precipitation magnitude increases, which also aligns with earlier studies (e.g., Castillo

et al., 2003; Nikolopoulos et al., 2011; Noto et al., 2008; Wood et al., 1990). Our study further emphasizes precipitation forecast as the primary source of uncertainty in flood forecasting. This finding agrees with previous research (e.g., Vincendon et al., 2011; Wu et al., 2020), and underscores the importance of accurate precipitation forecast, which can be more reliably achieved through an ensemble simulation instead of a deterministic one. Moreover, this study points out the necessity of model spin-up based on “practical” equilibrium to minimize the uncertainty associated with model initialization.

## ACKNOWLEDGEMENTS

Any use of trade, firm, or products names is for descriptive purposes only and does not imply endorsement by the U.S. Government.

## DATA AVAILABILITY STATEMENT

The data that support the findings of this study are available from the corresponding author upon reasonable request. The peak streamflow data are available from the U.S. Geological Survey (2022).

## ORCID

Dongxiao Yin  <https://orcid.org/0000-0002-4951-0066>

Z. George Xue  <https://orcid.org/0000-0003-4018-0248>

Yongjie Huang  <https://orcid.org/0000-0001-7883-8768>

## REFERENCES

- Abbaszadeh, P., Gavahi, K., & Moradkhani, H. (2020). Multivariate remotely sensed and in-situ data assimilation for enhancing community WRF-hydro model forecasting. *Advances in Water Resources*, 145, 103721. <https://doi.org/10.1016/J.ADVWATRES.2020.103721>
- Ajami, H., McCabe, M. F., & Evans, J. P. (2015). Impacts of model initialization on an integrated surface water-groundwater model. *Hydrological Processes*, 29(17), 3790–3801. <https://doi.org/10.1002/hyp.10478>
- Ajami, H., McCabe, M. F., Evans, J. P., & Stisen, S. (2014). Assessing the impact of model spin-up on surface water-groundwater interactions using an integrated hydrologic model. *Water Resources Research*, 50(3), 2636–2656. <https://doi.org/10.1002/2013WR014258>
- Bao, J. W., Michelson, S. A., & Grell, E. D. (2019). Microphysical process comparison of three microphysics parameterization schemes in the WRF model for an idealized squall-line case study. *Monthly Weather Review*, 147(9), 3093–3120. <https://doi.org/10.1175/MWR-D-18-0249.1>
- Bartalis, Z., Wagner, W., & Naeimi, V. (2007). Initial soil moisture retrievals from the METOP-A Advanced Scatterometer (ASCAT).

- Geophysical Research Letters, 34(20), 1–5. <https://doi.org/10.1029/2007GL031088>
- Berthet, L., Andréassian, V., Perrin, C., & Javelle, P. (2009). How crucial is it to account for the antecedent moisture conditions in flood forecasting? Comparison of event-based and continuous approaches on 178 catchments. *Hydrology and Earth System Sciences*, 13(6), 819–831. <https://doi.org/10.5194/hess-13-819-2009>
- Bowman, A. L., Franz, K. J., Hogue, T. S., & Kinoshita, A. M. 2015. MODIS-based potential evapotranspiration demand curves for the sacramento soil moisture accounting model. [https://doi.org/10.1061/\(ASCE\)JSTAR.2017.2651140](https://doi.org/10.1061/(ASCE)JSTAR.2017.2651140)
- Brocca, L., Crow, W. T., Ciabatta, L., Massari, C., De Rosnay, P., Enenkel, M., Hahn, S., Amarnath, G., Camici, S., Tarpanelli, A., & Wagner, W. (2017). A review of the applications of ASCAT soil moisture products. *IEEE Journal of Selected Topics in Applied Earth Observations and Remote Sensing*, 10(5), 2285–2306. <https://doi.org/10.1109/JSTARS.2017.2651140>
- Brocca, L., Melone, F., & Moramarco, T. (2008). On the estimation of antecedent wetness conditions in rainfall-runoff modelling. *Hydrological Processes*, 22(5), 629–642. <https://doi.org/10.1002/HYP.6629>
- Cai, X., Yang, Z. L., David, C. H., Niu, G. Y., & Rodell, M. (2014). Hydrological evaluation of the noah-MP land surface model for the Mississippi River basin. *Journal of Geophysical Research*, 119(1), 23–38. <https://doi.org/10.1002/2013JD020792>
- Castillo, V. M., Gómez-Plaza, A., & Martínez-Mena, M. (2003). The role of antecedent soil water content in the runoff response of semiarid catchments: A simulation approach. *Journal of Hydrology*, 284(1–4), 114–130. [https://doi.org/10.1016/S0022-1694\(03\)00264-6](https://doi.org/10.1016/S0022-1694(03)00264-6)
- Chen, T. H., Henderson-Sellers, A., Milly, P. C. D., Pitman, A. J., Beljaars, A. C. M., Polcher, J., Abramopoulos, F., Boone, A., Chang, S., Chen, F., Dai, Y., Desborough, C. E., Dickinson, R. E., Dumenil, L., E. k., M., Garratt, J. R., Gedney, N., Gusev, Y. M., Kim, J., ... Zeng, Q. (1997). Cabauw experimental results from the project for intercomparison of land-surface parameterization schemes. *Journal of Climate*, 10(6), 1194–1215. [https://doi.org/10.1175/1520-0442\(1997\)010<1194:CERFTP>2.0.CO;2](https://doi.org/10.1175/1520-0442(1997)010<1194:CERFTP>2.0.CO;2)
- Cosgrove, B. A., Lohmann, D., Mitchell, K. E., Houser, P. R., Wood, E. F., Schaake, J. C., Robock, A., Sheffield, J., Duan, Q., Luo, L., Higgins, R., Pinker, R. T., & Tarpley, J. D. (2003). Land surface model spin-up behavior in the North American land data assimilation system (NLDAS). *Journal of Geophysical Research: Atmospheres*, 108(22), 1–19. <https://doi.org/10.1029/2002jd003316>
- Diakakis, M. (2012). Rainfall thresholds for flood triggering. The case of Marathonas in Greece. *Natural Hazards*, 60(3), 789–800. <https://doi.org/10.1007/s11069-011-9904-7>
- Dinan, T. (2017). Projected increases in hurricane damage in the United States: The role of climate change and coastal development. *Ecological Economics*, 138, 186–198. <https://doi.org/10.1016/j.ecolecon.2017.03.034>
- Edouard, S., Vincendon, B., & Ducrocq, V. (2018). Ensemble-based flash-flood modelling: Taking into account hydrodynamic parameters and initial soil moisture uncertainties. *Journal of Hydrology*, 560, 480–494. <https://doi.org/10.1016/j.jhydrol.2017.04.048>
- Entekhabi, D., Njoku, E. G., O'Neill, P. E., Kellogg, K. H., Crow, W. T., Edelstein, W. N., Entin, J. K., Goodman, S. D., Jackson, T. J., Johnson, J., Kimball, J., Piepmeier, J. R., Koster, R. D., Martin, N., McDonald, K. C., Moghaddam, M., Moran, S., Reichle, R., Shi, J. C., ... Van Zyl, J. (2010). The soil moisture active passive (SMAP) mission. *Proceedings of the IEEE*, 98(5), 704–716. <https://doi.org/10.1109/JPROC.2010.2043918>
- Feaster, T. D., Weaver, J. C., Gotvald, A. J., Kolb, K. R. 2018. Preliminary peak stage and streamflow data for selected U.S. Geological Survey streamgaging stations in north and South Carolina for flooding following hurricane Florence, September 2018. Open-File Report 2018-1172 (October). <https://doi.org/10.3133/ofr20181172>
- Gochis, D., Barlage, M., Cabell, R., Casali, M., Dugger, A., FitzGerald, K., McAllister, M., McCreight, J., RafieeiNasab, A., Read, L., Sampson, K., Yates, D., & Zhang, Y. 2020. The WRF-hydro modeling system technical description, (Version 5.1.1) [https://ral.ucar.edu/sites/default/files/public/projects/wrf\\_hydro/technical-description-user-guide/wrf-hydro-v5.1.1-technical-description.pdf](https://ral.ucar.edu/sites/default/files/public/projects/wrf_hydro/technical-description-user-guide/wrf-hydro-v5.1.1-technical-description.pdf).
- Grillakis, M. G., Koutoulis, A. G., Komma, J., Tsanis, I. K., Wagner, W., & Blöschl, G. (2016). Initial soil moisture effects on flash flood generation – A comparison between basins of contrasting hydro-climatic conditions. *Journal of Hydrology*, 541, 206–217. <https://doi.org/10.1016/j.jhydrol.2016.03.007>
- Gu, L., Meyers, T., Pallardy, S. G., Hanson, P. J., Yang, B., Heuer, M., Hosman, K. P., Riggs, J. S., Sluss, D., & Wullschleger, S. D. (2006). Direct and indirect effects of atmospheric conditions and soil moisture on surface energy partitioning revealed by a prolonged drought at a temperate forest site. *Journal of Geophysical Research Atmospheres*, 111(16), 1–13. <https://doi.org/10.1029/2006JD007161>
- Hamel, P., & Guswa, A. J. (2015). Uncertainty analysis of a spatially explicit annual water-balance model: Case study of the cape fear basin, North Carolina. *Hydrology and Earth System Sciences*, 19(2), 839–853. <https://doi.org/10.5194/hess-19-839-2015>
- Hersbach, H., Bell, B., Berrisford, P., Hirahara, S., Horányi, A., Muñoz-Sabater, J., Nicolas, J., Peubey, C., Radu, R., Schepers, D., Simmons, A., Soci, C., Abdalla, S., Abellan, X., Balsamo, G., Bechtold, P., Biavati, G., Bidlot, J., Bonavita, M., ... Thépaut, J. N. (2020). The ERA5 global reanalysis. *Quarterly Journal of the Royal Meteorological Society*, 146(730), 1999–2049. <https://doi.org/10.1002/qj.3803>
- Hewlett, J. D., Fortson, J. C., & Cunningham, G. B. (1977). The effect of rainfall intensity on storm flow and peak discharge from forest land. *Water Resources Research*, 13(2), 259–266. <https://doi.org/10.1029/WR013i002p00259>
- Hong, S., Lim, K., Kim, J., Lim, J. J., & Dudhia, J. 2005. WRF Single-Moment 6-Class Microphysics Scheme (WSM6). pp. 5–6.
- Hong, S. Y., Noh, Y., & Dudhia, J. (2006). A new vertical diffusion package with an explicit treatment of entrainment processes. *Monthly Weather Review*, 134(9), 2318–2341. <https://doi.org/10.1175/MWR3199.1>
- Hsiao, L. F., Yang, M. J., Lee, C. S., Kuo, H. C., Shih, D. S., Tsai, C. C., Wang, C. J., Chang, L. Y., Chen, D. Y. C., Feng, L., Hong, J. S., Fong, C. T., Chen, D. S., Yeh, T. C., Huang, C. Y., Guo, W. D., & Lin, G. F. (2013). Ensemble forecasting of typhoon rainfall and floods over a mountainous watershed in Taiwan. *Journal of Hydrology*, 506, 55–68. <https://doi.org/10.1016/j.jhydrol.2013.08.046>
- Huang, J. C., Yu, C. K., Lee, J. Y., Cheng, L. W., Lee, T. Y., & Kao, S. J. (2012). Linking typhoon tracks and spatial rainfall patterns for improving flood lead time predictions over a mesoscale mountainous watershed. *Water Resources Research*, 48(9), 1–15. <https://doi.org/10.1029/2011WR011508>
- Iacono, M. J., Delamere, J. S., Mlawer, E. J., Shephard, M. W., Clough, S. A., & Collins, W. D. (2008). Radiative forcing by long-lived greenhouse gases: Calculations with the AER radiative transfer models. *Journal of Geophysical Research Atmospheres*, 113(13), 2–9. <https://doi.org/10.1029/2008JD009944>
- Kendon, E. J., Roberts, N. M., Senior, C. A., & Roberts, M. J. (2012). Realism of rainfall in a very high-resolution regional climate model. *Journal of Climate*, 25(17), 5791–5806. <https://doi.org/10.1175/JCLI-D-11-00562.1>
- Kerandi, N., Arnault, J., Laxu, P., Wagner, S., Kitheka, J., & Kunstmann, H. (2018). Joint atmospheric-terrestrial water balances for East Africa: A WRF-hydro case study for the upper Tana River basin. *Theoretical and Applied Climatology*, 131(3–4), 1337–1355. <https://doi.org/10.1007/s00704-017-2050-8>
- Klongvessa, P., Lu, M., & Chotpantarat, S. (2018). Response of the flood peak to the spatial distribution of rainfall in the Yom River basin, Thailand. *Stochastic Environmental Research and Risk Assessment*, 32(10), 2871–2887. <https://doi.org/10.1007/s00477-018-1603-4>

- Knutson, T. R., McBride, J. L., Chan, J., Emanuel, K., Holland, G., Landsea, C., Held, I., Kossin, J. P., Srivastava, A. K., & Sugi, M. (2010). Tropical cyclones and climate change. *Nature Geoscience*, 3(3), 157–163. <https://doi.org/10.1038/ngeo779>
- Komma, J., Blöschl, G., & Reszler, C. (2008). Soil moisture updating by ensemble Kalman filtering in real-time flood forecasting. *Journal of Hydrology*, 357(3–4), 228–242. <https://doi.org/10.1016/J.JHYDROL.2008.05.020>
- Komma, J., Reszler, C., Blöschl, G., & Haiden, T. (2007). Ensemble prediction of floods – catchment non-linearity and forecast probabilities. *Natural Hazards and Earth System Sciences*, 7(4), 431–444. <https://doi.org/10.5194/NHESS-7-431-2007>
- Kunkel, K. E., & Champion, S. M. (2019). An assessment of rainfall from hurricanes Harvey and Florence relative to other extremely wet storms in the United States. *Geophysical Research Letters*, 46(22), 13500–13506. <https://doi.org/10.1029/2019GL085034>
- Li, L., Gochis, D. J., Sobolowski, S., & Mesquita, M. D. S. (2017). Evaluating the present annual water budget of a Himalayan headwater river basin using a high-resolution atmosphere-hydrology model. *Journal of Geophysical Research*, 122(9), 4786–4807. <https://doi.org/10.1002/2016JD026279>
- Li, L., Pontoppidan, M., Sobolowski, S., & Senatore, A. (2020). The impact of initial conditions on convection-permitting simulations of a flood event over complex mountainous terrain. *Hydrology and Earth System Sciences*, 24(2), 771–791. <https://doi.org/10.5194/hess-24-771-2020>
- Li, X., Zhao, G., Nielsen-Gammon, J., Salazar, J., Wigmosta, M., Sun, N., Judi, D., & Gao, H. (2020). Impacts of urbanization, antecedent rainfall event, and cyclone tracks on extreme floods at Houston reservoirs during hurricane Harvey. *Environmental Research Letters*, 15(12), 1–10. <https://doi.org/10.1088/1748-9326/abc4ff>
- Lin, P., Hopper, L. J., Yang, Z.-L., Lenz, M., & Zeitler, J. W. (2018). Insights into hydrometeorological factors constraining flood prediction skill during the May and October 2015 Texas Hill country flood events. *Journal of Hydrometeorology*, 19(8), 1339–1361. <https://doi.org/10.1175/jhm-d-18-0038.1>
- Lin, P., Rajib, M. A., Yang, Z. L., Somos-Valenzuela, M., Merwade, V., Maidment, D. R., Wang, Y., & Chen, L. (2018). Spatiotemporal evaluation of simulated evapotranspiration and streamflow over Texas using the WRF-hydro-RAPID modeling framework. *Journal of the American Water Resources Association*, 54(1), 40–54. <https://doi.org/10.1111/1752-1688.12585>
- Lin, Y. (2011). GCIP/EOP surface: Precipitation NCEP/EMC 4KM gridded data (GRIB) stage IV data. Version 1.0. <https://doi.org/10.5065/D6PG1QDD>.
- Liu, L., Gao, C., Xuan, W., & Xu, Y. P. (2017). Evaluation of medium-range ensemble flood forecasting based on calibration strategies and ensemble methods in Lanjiang Basin, Southeast China. *Journal of Hydrology*, 554, 233–250. <https://doi.org/10.1016/j.jhydrol.2017.08.032>
- Mackey, B. P., & Krishnamurti, T. N. (2001). Ensemble forecast of a typhoon flood event. *Weather and Forecasting*, 16(4), 399–415. [https://doi.org/10.1175/1520-0434\(2001\)016<0399:EFOATF>2.0.CO;2](https://doi.org/10.1175/1520-0434(2001)016<0399:EFOATF>2.0.CO;2)
- Massari, C., Brocca, L., Barbetta, S., Papathanasiou, C., Mimikou, M., & Moramarco, T. (2014). Using globally available soil moisture indicators for flood modelling in mediterranean catchments. *Hydrology and Earth System Sciences*, 18(2), 839–853. <https://doi.org/10.5194/HESS-18-839-2014>
- Massari, C., Brocca, L., Moramarco, T., Tramblay, Y., & Didon Lescot, J. F. (2014). Potential of soil moisture observations in flood modelling: Estimating initial conditions and correcting rainfall. *Advances in Water Resources*, 74, 44–53.
- Mcmillan, H., Gueguen, M., Grimon, E., Woods, R., Clark, M., & Rupp, D. E. (2014). Spatial variability of hydrological processes and model structure diagnostics in a 50km<sup>2</sup> catchment. *Hydrological Processes*, 28(18), 4896–4913. <https://doi.org/10.1002/HYP.9988>
- Miller, D. A., & White, R. A. (1998). A conterminous United States multi-layer soil characteristics dataset for regional climate and hydrology modeling. *Earth Interactions*, 2(1), 2. [https://doi.org/10.1175/1087-3562\(1998\)002<0002:cusms>2.0.co;2](https://doi.org/10.1175/1087-3562(1998)002<0002:cusms>2.0.co;2)
- Mitchell, K. E., Lohmann, D., Houser, P. R., Wood, E. F., Schaake, J. C., Robock, A., Cosgrove, B. A., Sheffield, J., Duan, Q., Luo, L., Higgins, R. W., Pinker, R. T., Tarpley, J. D., Lettenmaier, D., Marshall, C., Entin, J., Pan, M., Shi, W., Koren, V., ... Bailey, A. A. (2004). The multi-institution north American land data assimilation system (NLDAS): Utilizing multiple GCIP products and partners in a continental distributed hydrological modeling system. *Journal of Geophysical Research D: Atmospheres*, 109(7), 1–32. <https://doi.org/10.1029/2003jd003823>
- Morrison, H., Thompson, G., & Tatarki, V. (2009). Impact of cloud micro-physics on the development of trailing stratiform precipitation in a simulated squall line: Comparison of one- and two-moment schemes. *Monthly Weather Review*, 137(3), 991–1007. <https://doi.org/10.1175/2008MWR2556.1>
- Mu, Q., Zhao, M., & Running, S. W. (2011). Improvements to a MODIS global terrestrial evapotranspiration algorithm. *Remote Sensing of Environment*, 115(8), 1781–1800. <https://doi.org/10.1016/j.rse.2011.02.019>
- National Centers for Environmental Prediction/National Weather Service/NOAA/U.S. Department of Commerce. (2000). NCEP FNL operational model global tropospheric analyses, continuing from July 1999, research data archive at the National Center for Atmospheric Research, Computational and Information Systems. *The Laboratory*. <https://doi.org/10.5065/D6M043C6>
- Nester, T., Komma, J., Viglione, A., & Blöschl, G. (2012). Flood forecast errors and ensemble spread—a case study. *Water Resources Research*, 48(10), 1–19. <https://doi.org/10.1029/2011WR011649>
- Nikolopoulos, E. I., Anagnostou, E. N., Borga, M., Vivoni, E. R., & Papadopoulos, A. (2011). Sensitivity of a mountain basin flash flood to initial wetness condition and rainfall variability. *Journal of Hydrology*, 402(3–4), 165–178. <https://doi.org/10.1016/j.jhydrol.2010.12.020>
- Niu, G. Y., Yang, Z. L., Mitchell, K. E., Chen, F., Ek, M. B., Barlage, M., Kumar, A., Manning, K., Niyogi, D., Rosero, E., Tewari, M., & Xia, Y. (2011). The community Noah land surface model with multiparameterization options (Noah-MP): 1. Model description and evaluation with local-scale measurements. *Journal of Geophysical Research Atmospheres*, 116(12), 1–19. <https://doi.org/10.1029/2010JD015139>
- Noto, L. V., Ivanov, V. Y., Bras, R. L., & Vivoni, E. R. (2008). Effects of initialization on response of a fully-distributed hydrologic model. *Journal of Hydrology*, 352(1–2), 107–125. <https://doi.org/10.1016/j.jhydrol.2007.12.031>
- Ogden, F. L., & Julien, P. Y. (1993). Runoff sensitivity to temporal and spatial rainfall variability at runoff plane and small basin scales. *Water Resources Research*, 29(8), 2589–2597. <https://doi.org/10.1029/93WR00924>
- Oppel, H., & Fischer, S. (2020). A new unsupervised learning method to assess clusters of temporal distribution of rainfall and their coherence with flood types. *Water Resources Research*, 56(5), 1–16. <https://doi.org/10.1029/2019WR026511>
- Paerl, H. W., Hall, N. S., Hounshell, A. G., Luettich, R. A., Rossignol, K. L., Osburn, C. L., & Bales, J. (2019). Recent increase in catastrophic tropical cyclone flooding in coastal North Carolina, USA: Long-term observations suggest a regime shift. *Scientific Reports*, 9(1), 1–9. <https://doi.org/10.1038/s41598-019-46928-9>
- Pal, S., Chang, H.-I., Castro, C. L., & Dominguez, F. (2019). Credibility of convection-permitting modeling to improve seasonal precipitation forecasting in the southwestern United States. *Frontiers in Earth Science*, 0, 11. <https://doi.org/10.3389/FEART.2019.00011>
- Parajuli, P. B., Jayakody, P., & Ouyang, Y. (2018). Evaluation of using remote sensing evapotranspiration data in SWAT. *Water Resources Management*, 32(3), 985–996. <https://doi.org/10.1007/s11269-017-1850-z>

- Peng, J., Loew, A., Merlin, O., & Verhoest, N. E. C. (2017). A review of spatial downscaling of satellite remotely sensed soil moisture. *Reviews of Geophysics*, 55(2), 341–366. <https://doi.org/10.1002/2016RG000543>
- Penna, D., Tromp-Van Meerveld, H. J., Gobbi, A., Borga, M., & Dalla, F. G. (2011). The influence of soil moisture on threshold runoff generation processes in an alpine headwater catchment. *Hydrology and Earth System Sciences*, 15(3), 689–702. <https://doi.org/10.5194/hess-15-689-2011>
- Radatz, T. F., Thompson, A. M., & Madison, F. W. (2013). Soil moisture and rainfall intensity thresholds for runoff generation in southwestern Wisconsin agricultural watersheds. *Hydrological Processes*, 27(25), 3521–3534. <https://doi.org/10.1002/HYP.9460>
- Rappaport, E. N. (2014). Fatalities in the United States from Atlantic tropical cyclones: New data and interpretation. *Bulletin of the American Meteorological Society*, 95(3), 341–346. <https://doi.org/10.1175/BAMS-D-12-00074.1>
- Running, S., Mu, Q., & Zhao, M. MOD16A2 MODIS/Terra net evapotranspiration 8-day L4 global 500m SIN grid V006 [data set]. NASA EOSDIS Land Processes DAAC: n.d. <https://doi.org/10.5067/MODIS/MOD16A2.006>.
- Schröter, K., Kunz, M., Elmer, F., Mühr, B., & Merz, B. (2014). What made the June 2013 flood in Germany an exceptional event? A hydro-meteorological evaluation. *Hydrology and Earth System Sciences Discussions*, 11(7), 8125–8166. <https://doi.org/10.5194/hessd-11-8125-2014>
- Seck, A., Welty, C., & Maxwell, R. M. (2015). Spin-up behavior and effects of initial conditions for an integrated hydrologic model. *Water Resources Research*, 51(4), 2188–2210. <https://doi.org/10.1002/2014WR016371>
- Senatore, A., Davolio, S., Furnari, L., & Mendicino, G. (2020). Reconstructing flood events in mediterranean coastal areas using different reanalyses and high-resolution meteorological models. *Journal of Hydrometeorology*, 21(8), 1865–1887. <https://doi.org/10.1175/JHM-D-19-0270.1>
- Senatore, A., Furnari, L., & Mendicino, G. (2020). Impact of high-resolution sea surface temperature representation on the forecast of small Mediterranean catchments' hydrological responses to heavy precipitation. *Hydrology and Earth System Sciences*, 24(1), 269–291. <https://doi.org/10.5194/hess-24-269-2020>
- Sharma, A., Wasko, C., & Lettenmaier, D. P. (2018). If precipitation extremes are increasing, why aren't floods? *Water Resources Research*, 54(11), 8545–8551. <https://doi.org/10.1029/2018WR023749>
- Silvestro, F., & Rebora, N. (2014). Impact of precipitation forecast uncertainties and initial soil moisture conditions on a probabilistic flood forecasting chain. *Journal of Hydrology*, 519(PA), 1052–1067. <https://doi.org/10.1016/j.jhydrol.2014.07.042>
- Singh, V. P. (1997). Effect of spatial and temporal variability in rainfall and watershed characteristics on stream flow hydrograph. *Hydrological Processes*, 11(12), 1649–1669. [https://doi.org/10.1002/\(SICI\)1099-1085\(19971015\)11:12<1649::AID-HYP495>3.0.CO;2-1](https://doi.org/10.1002/(SICI)1099-1085(19971015)11:12<1649::AID-HYP495>3.0.CO;2-1)
- Smith, J. A., Baeck, M. L., Villarini, G., & Krajewski, W. F. (2010). The hydrology and hydrometeorology of flooding in the Delaware River basin. *Journal of Hydrometeorology*, 11(4), 841–859. <https://doi.org/10.1175/2010JHM1236.1>
- Smith, J. A., Sturdevant-Rees, P., Baeck, M. L., & Larsen, M. C. (2005). Tropical cyclones and the flood hydrology of Puerto Rico. *Water Resources Research*, 41(6), 1–16. <https://doi.org/10.1029/2004WR003530>
- Somos-Valenzuela, M. A., & Palmer, R. N. (2018). Use of WRF-hydro over the northeast of the US to estimate water budget tendencies in small watersheds. *Water (Switzerland)*, 10(12), 1–17. <https://doi.org/10.3390/w10121709>
- Stewart, S. R.. (2017). Hurricane Matthew. National Hurricane Center (October 2016). 1–96. [http://www.nhc.noaa.gov/data/tcr/AL142016\\_Matthew.pdf](http://www.nhc.noaa.gov/data/tcr/AL142016_Matthew.pdf)
- Stewart, S. R., & Berg, R. (2019). National hurricane center tropical cyclone report. Hurricane Florence. (May). 1–98.
- Sturdevant-Rees, P., Smith, J. A., Morrison, J., & Baeck, M. L. (2001). Tropical storms and the flood hydrology of the Central Appalachians. *Water Resources Research*, 37(8), 2143–2168. <https://doi.org/10.1029/2000WR900310>
- Thompson, G., Field, P. R., Rasmussen, R. M., & Hall, W. D. (2008). Explicit forecasts of winter precipitation using an improved bulk microphysics scheme. Part II: Implementation of a new snow parameterization. *Monthly Weather Review*, 136(12), 5095–5115. <https://doi.org/10.1175/2008MWR2387.1>
- Tiedtke, M. (1989). A comprehensive mass flux scheme for cumulus parameterization in large-scale models. *Monthly Weather Review*, 117, 1779–1800.
- Tolson, B. A., & Shoemaker, C. A. (2007). Dynamically dimensioned search algorithm for computationally efficient watershed model calibration. *Water Resources Research*, 43(1), 1–16. <https://doi.org/10.1029/2005WR004723>
- U.S. Geological Survey. (2022). USGS water data for the nation: U.S. Geological Survey National Water Information System database.
- Uber, M., Vandervaere, J. P., Zin, I., Braud, I., Heistermann, M., Legouët, C., Molinié, G., & Nord, G. (2018). How does initial soil moisture influence the hydrological response? A case study from southern France. *Hydrology and Earth System Sciences*, 22(12), 6127–6146. <https://doi.org/10.5194/hess-22-6127-2018>
- UCAR. (2019). WRF - Weather Research & Forecasting Model. (January). 1–456.
- Villarini, G., & Smith, J. A. (2010). Flood peak distributions for the eastern United States. *Water Resources Research*, 46(6), 1–17. <https://doi.org/10.1029/2009WR008395>
- Villarini, G., Smith, J. A., Baeck, M. L., Marchok, T., & Vecchi, G. A. (2011). Characterization of rainfall distribution and flooding associated with U.S. landfalling tropical cyclones: Analyses of hurricanes Frances, Ivan, and Jeanne (2004). *Journal of Geophysical Research Atmospheres*, 116(23), 1–19. <https://doi.org/10.1029/2011JD016175>
- Vincendon, B., Ducrocq, V., Nuissier, O., & Vié, B. (2011). Perturbation of convection-permitting NWP forecasts for flash-flood ensemble forecasting. *Natural Hazards and Earth System Science*, 11(5), 1529–1544. <https://doi.org/10.5194/nhess-11-1529-2011>
- Vogel, H. J., Hoffmann, H., Leopold, A., & Roth, K. (2005). Studies of crack dynamics in clay soil: II. A physically based model for crack formation. *Geoderma*, 125(3–4), 213–223. <https://doi.org/10.1016/J.GEODERMA.2004.07.008>
- Vogel, H. J., Hoffmann, H., & Roth, K. (2005). Studies of crack dynamics in clay soil: I. experimental methods, results, and morphological quantification. *Geoderma*, 125(3–4), 203–211. <https://doi.org/10.1016/J.GEODERMA.2004.07.009>
- Walsh, K. J. E., McBride, J. L., Klotzbach, P. J., Balachandran, S., Camargo, S. J., Holland, G., Knutson, T. R., Kossin, J. P., Lee, T., Sobel, A., & Sugi, M. (2016). Tropical cyclones and climate change. *Wiley Interdisciplinary Reviews: Climate Change*, 7(1), 65–89. <https://doi.org/10.1002/wcc.371>
- Wing, O. E. J., Bates, P. D., Smith, A. M., Sampson, C. C., Johnson, K. A., Fargione, J., & Morefield, P. (2018). Estimates of present and future flood risk in the conterminous United States. *Environmental Research Letters*, 13(3), 1–7. <https://doi.org/10.1088/1748-9326/aaac65>
- Wood, A. W., & Lettenmaier, D. P. (2008). An ensemble approach for attribution of hydrologic prediction uncertainty. *Geophysical Research Letters*, 35(14), 1–5. <https://doi.org/10.1029/2008GL034648>
- Wood, E. F., Sivapalan, M., & Beven, K. (1990). Similarity and scale in catchment response. *Reviews of Geophysics*, 28(89), 1–18.
- Woodhams, B. J., Birch, C. E., Marsham, J. H., Bain, C. L., Roberts, N. M., & Boyd, D. F. A. (2018). What is the added value of a convection-permitting model for forecasting extreme rainfall over tropical East

- Africa? *Monthly Weather Review*, 146(9), 2757–2780. <https://doi.org/10.1175/MWR-D-17-0396.1>
- Wu, W., Emerton, R., Duan, Q., Wood, A. W., Wetterhall, F., & Robertson, D. E. (2020). Ensemble flood forecasting: Current status and future opportunities. *WIREs Water*, 7(3), 1–32. <https://doi.org/10.1002/wat2.1432>
- Xia, Y., Mitchell, K., Ek, M., Sheffield, J., Cosgrove, B., Wood, E., Luo, L., Alonge, C., Wei, H., Meng, J., Livneh, B., Lettenmaier, D., Koren, V., Duan, Q., Mo, K., Fan, Y., & Mocko, D. (2012). Continental-scale water and energy flux analysis and validation for the north American land data assimilation system project phase 2 (NLDAS-2): 1. Intercomparison and application of model products. *Journal of Geophysical Research Atmospheres*, 117(3), 1–27. <https://doi.org/10.1029/2011JD016048>
- Xue, Z. G., Gochis, D. J., Yu, W., Keim, B. D., Rohli, R. V., Zang, Z., Sampson, K., Dugger, A., Sathiaraj, D., & Ge, Q. (2018). Modeling hydroclimatic change in Southwest Louisiana rivers. *Water (Switzerland)*, 10(5), 1–20. <https://doi.org/10.3390/w10050596>
- Yang, L., Liu, M., Smith, J. A., & Tian, F. (2017). Typhoon nina and the august 1975 flood over Central China. *Journal of Hydrometeorology*, 18(2), 451–472. <https://doi.org/10.1175/JHM-D-16-0152.1>
- Yang, Z. L., Dickinson, R. E., Henderson-Selles, A., & Pitman, A. J. (1995). Preliminary study of spin-up processes in land surface models with the first stage data of project for intercomparison of land surface parameterization schemes phase 1(a). *Journal of Geophysical Research*, 100(D8), 16553–16578. <https://doi.org/10.1029/95jd01076>
- Yin, D., Xue, Z. G., Gochis, D. J., Yu, W., Morales, M., & Rafieeinab, A. (2020). A process-based, fully distributed soil erosion and sediment transport model for WRF-hydro. *Water (Switzerland)*, 12(6), 1–23. <https://doi.org/10.3390/w12061840>
- Yin, D., Xue, Z. G., Warner, J. C., Bao, D., Huang, Y., & Yu, W. (2021). Hydrometeorology and hydrology of flooding in cape fear river basin during hurricane Florence in 2018. *Journal of Hydrology*, 603, 127139. <https://doi.org/10.1016/J.JHYDROL.2021.127139>
- Yucel, I., Onen, A., Yilmaz, K. K., & Gochis, D. J. (2015). Calibration and evaluation of a flood forecasting system: Utility of numerical weather prediction model, data assimilation and satellite-based rainfall. *Journal of Hydrology*, 523, 49–66. <https://doi.org/10.1016/j.jhydrol.2015.01.042>
- Zehe, E., & Sivapalan, M. (2009). Threshold behaviour in hydrological systems as (human) geo-ecosystems: Manifestations, controls, implications. *Hydrology and Earth System Sciences*, 13(7), 1273–1297. <https://doi.org/10.5194/hess-13-1273-2009>
- Zhang, C., Wang, Y., & Hamilton, K. (2011). Improved representation of boundary layer clouds over the southeast pacific in ARW-WRF using a modified tiedtke cumulus parameterization scheme. *Monthly Weather Review*, 139(11), 3489–3513. <https://doi.org/10.1175/MWR-D-10-0509.1>

## SUPPORTING INFORMATION

Additional supporting information can be found online in the Supporting Information section at the end of this article.

**How to cite this article:** Yin, D., Xue, Z. G., Bao, D., Rafieeinab, A., Huang, Y., Morales, M., & Warner, J. C. (2022). Understanding the role of initial soil moisture and precipitation magnitude in flood forecast using a hydrometeorological modelling system. *Hydrological Processes*, 36(10), e14710. <https://doi.org/10.1002/hyp.14710>